

# Closed Universes, de Sitter Space and Inflation

Anthony Lasenby<sup>1</sup> and Chris Doran<sup>2</sup>

Astrophysics Group, Cavendish Laboratory, Madingley Road,  
Cambridge CB3 0HE, UK.

## Abstract

Experimental evidence points firmly to the existence of some form of dark energy in the universe. The simplest explanation for this is the existence of a cosmological constant, which encourages the consideration of spatially closed universes of de Sitter type. Conformal embedding in a de Sitter background suggests a boundary condition for cosmological models, which can explain the size of the cosmological constant. For this boundary condition to give rise to physically acceptable models an inflationary period is required. Contrary to some claims in the literature, we show that it is quite straightforward to construct consistent models of inflation in a closed universe. The models require no fine tuning, except in the mass of the scalar field. Our theory naturally predicts the observed values of the cosmological parameters and fits the WMAP data extremely well. The primordial curvature spectrum predicts the low- $\ell$  fall-off in the CMB power spectrum observed by WMAP. The spectrum also predicts a fall-off in the matter spectrum at high  $k$ , relative to a power law.

PACS numbers: 98.80.Cq, 98.80.Jk, 98.80.Es, 04.20.Gz

## 1 Introduction

Experimental evidence for the existence of a cosmological constant has grown dramatically over recent years. It now seems likely that the cosmological constant, or some form of ‘dark energy’, is responsible for around 70% of the total energy density of the universe [1]. Despite this, the cosmological constant is often treated as a rather unwelcome addition to the Friedmann–Robertson–Walker (FRW) equations. One reason for this is the popular belief that the cosmological constant is not fundamental, but is a relic from symmetry breaking in a more complete theory. As is well known, the problem with such an idea is that the scale of the cosmological constant is hard to explain. Indeed, the fact that the energy density in the cosmological constant is currently of the same order as that of the large scale matter density suggests that the origin of the constant is related to the large scale geometry of the universe. Here we develop the geometric viewpoint, and suggest a novel boundary condition which can account for the size of the cosmological constant.

The first idea we investigate is the relationship between the cosmological constant and the flatness problem. By plotting the evolution of various cosmological models in the  $\Omega_M$ – $\Omega_\Lambda$  plane we see that the majority of models converge to the spatially-flat case for a wide range of initial conditions. This is quite distinct to the case with no cosmological constant, where any slight deviation

---

<sup>1</sup>e-mail: a.n.lasenby@mrao.cam.ac.uk

<sup>2</sup>e-mail: c.Doran@mrao.cam.ac.uk

from spatial flatness quickly grows, requiring severe fine-tuning of the initial conditions. The flatness problem is less of an issue in models containing a  $\Lambda$  term, though this observation is strangely neglected in the literature.

We next investigate some properties of de Sitter geometry, and present a novel picture of this geometry that generalises the Poincaré disk picture of hyperbolic geometry [2, 3]. If we insist that any cosmological field can be described by fields that fully cover de Sitter space (with the fields singular at  $t = 0$ ) we arrive at a boundary condition which removes a degree of freedom from the model. This condition states that the total amount of conformal time available to the universe should equal  $\pi/2$ . For a simple dust cosmology this boundary condition singles out a model which predicts a universe that is closed at around the 10% level. The boundary condition therefore predicts a value of  $\Lambda$  which is of the correct order of magnitude for cosmological models, although this precise model is ruled out by the WMAP data [1].

An unusual feature of our boundary condition is that it rests on the behaviour of the universe at late times, rather than at the initial singularity. This may seem uncomfortable from the point of view of causality, but it is perfectly sound from the viewpoint of wave mechanics. In field theory one regularly applies boundary conditions at temporal infinity, and the model presented here extends this idea to the universe. Furthermore, our model has a number of attractive features from the point of view of conformal representations of cosmological models [4].

We next apply the same reasoning to an inflationary model in which the universe is filled by a single scalar field with a quadratic potential. We only consider the case of a massive scalar field as this is the most economic model which involves the least new physics. In order to apply our boundary condition we need to study the evolution of the scalar field from the initial singularity, through the inflationary region, before matching onto a standard cosmological model. Expanding the field equations around the initial singularity involves a complicated iterative scheme that can be extended to arbitrary precision. The series is governed by two parameters, which effectively control the degree of inflation and the curvature. Fixing both of these parameters to be of order unity produces inflationary models in a closed universe which are consistent with observation. This refutes the claim that it is difficult to obtain closed universe inflation without excessive fine tuning [5, 6, 7, 8, 9].

As the universe exits the inflationary region it evolves as if it had started from an effective big-bang, with a displaced time coordinate. Photons have travelled an appreciable distance by the end of inflation, which alters the boundary conditions we need to apply. The result of these effects is the imposition of a see-saw mechanism linking the current state of the universe and the initial conditions. The more we increase the number of e-folds during inflation, the smaller the value of the cosmological constant, and vice-versa. With initial conditions chosen to give the required number of e-foldings to generate the observed perturbation spectrum, we find that the predicted universe is closed at the level of a few percent. Given a present value of  $\Omega_M$  at around 0.3 we single out models with  $\Omega_\Lambda \approx 0.7$ . That is, the boundary condition predicts both the degreee of flatness of the universe and the magnitude of the cosmological constant.

A further attractive feature of this model is seen when we study the growth of perturbations. The primordial curvature spectrum we predict shows a strong departure from a simple power law, with an exponential cut-off at low wave

number, and an additional fall-off at high  $k$ . The resulting CMB power spectrum is in good agreement with the WMAP data [1], and is able to explain the observed low- $\ell$  deficit. We end with a discussion of the various issues raised in this paper, as well as an outline of future work.

Unless stated otherwise we work in units where  $G = c = \hbar = 1$ . Where it adds clarity, factors of  $G$  are included, so that  $G$  has dimensions of (distance)<sup>2</sup>.

## 2 Cosmological Evolution

The FRW equations, with  $c = 1$ , are

$$\frac{\dot{R}^2 + k}{R^2} - \frac{\Lambda}{3} = \frac{8\pi G}{3}\rho, \quad (1)$$

$$2\frac{\ddot{R}}{R} + \frac{\dot{R}^2 + k}{R^2} - \Lambda = -8\pi G P, \quad (2)$$

where  $k = 0, \pm 1$ . The scale parameter  $R$  is chosen to have explicit dimensions of distance. This is more appropriate when considering closed universe models, which we concentrate on in this paper. Rather than work directly with the scale parameter  $R$ , it is more convenient to express these equations in terms of  $\Omega_M$  and  $\Omega_\Lambda$ , which define the ratios of the total matter density and cosmological constant to their values for ensuring that the universe is spatially flat. We set

$$\Omega_M = \frac{8\pi G\rho}{3H^2} \quad (3)$$

$$\Omega_\Lambda = \frac{\Lambda}{3H^2} \quad (4)$$

where the Hubble function  $H$  is defined by

$$H = \frac{\dot{R}}{R}. \quad (5)$$

The universe is spatially flat if  $\Omega_M + \Omega_\Lambda = 1$ .

In order to consider various equations of state we first write the pressure  $P$  as

$$P = \eta\rho. \quad (6)$$

The variables  $\Omega_M$  and  $\Omega_\Lambda$  then satisfy the first-order equations

$$\frac{d\Omega_M}{dt} = H\Omega_M((1+3\eta)(\Omega_M - 1) - 2\Omega_\Lambda) \quad (7)$$

and

$$\frac{d\Omega_\Lambda}{dt} = H\Omega_\Lambda((1+3\eta)\Omega_M - 2\Omega_\Lambda + 2). \quad (8)$$

Dividing these we arrive at the equation

$$\frac{d\Omega_\Lambda}{d\Omega_M} = \frac{\Omega_\Lambda((1+3\eta)\Omega_M - 2(\Omega_\Lambda - 1))}{\Omega_M((1+3\eta)(\Omega_M - 1) - 2\Omega_\Lambda)}. \quad (9)$$

This equation defines a series of flow lines in the  $\Omega_M$ – $\Omega_\Lambda$  plane. The equation also highlights the significance of the points  $(1, 0)$  and  $(0, 1)$  in this plane. These

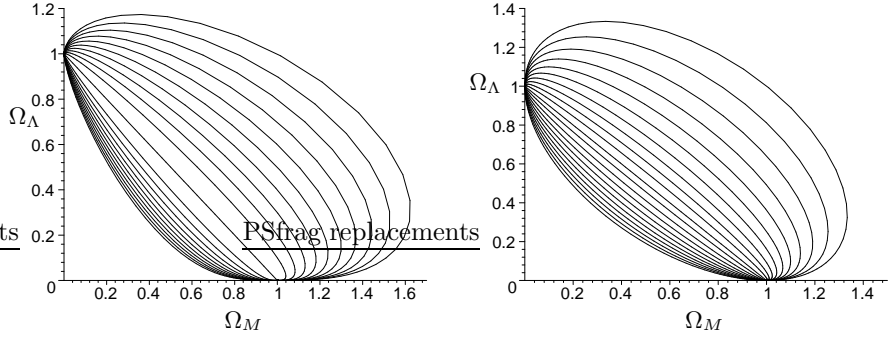


Figure 1: Evolution curves in the  $\Omega_M$ – $\Omega_\Lambda$  plane. The left-hand plot is for dust, and the right-hand plot is for radiation. In both cases the curves converge to  $\Omega_\Lambda = 1$ , representing a late-time de Sitter phase.

points act as attractors of the flow lines. This behaviour is illustrated in figure 1, which shows a series of flow lines starting from  $\Omega_M = 1$ ,  $\Omega_\Lambda = 0$ . The two plots are for the case of dust ( $\eta = 0$ ) and radiation ( $\eta = 1/3$ ). Seeding the plots around  $\Omega_M = 1$  is aided by the expansion

$$\Omega_\Lambda \approx A|\Omega_M - 1|^{(3(1+\eta)/(1+3\eta))}, \quad (10)$$

which assumes that  $\eta$  is roughly constant around  $\Omega_M = 1$ . The expansion is governed by a single parameter  $A$ , which fixes the behaviour of the curve at  $\Omega_M = 1$ . This parameter therefore controls the future evolution of the universe. The plots shown in figure 1 show  $A$  values in the range from 1 to 100, and the limit  $A \mapsto \infty$  corresponds to spatially flat. Recollapse (for radiation models) requires  $A < 1/4$ , and in this case the flow lines move out a finite distance before turning back on themselves.

An alternative version of the equations, more useful in describing the universe since recombination, is to assume that the matter density is made up of decoupled dust and radiation. Writing the densities of these as  $\rho_m$  and  $\rho_r$  respectively, we introduce the quantities

$$\Omega_m = \frac{8\pi G \rho_m}{3H^2}, \quad \text{and} \quad \Omega_r = \frac{8\pi G \rho_r}{3H^2}. \quad (11)$$

Since the matter and radiation are decoupled, both stress-energy tensors satisfy separate conservation laws, which reduce to

$$\rho_m R^3 = \text{constant}, \quad \text{and} \quad \rho_r R^4 = \text{constant}. \quad (12)$$

For this case we find that the equations governing  $\Omega_\Lambda$ ,  $\Omega_m$  and  $\Omega_r$  can be solved exactly, with the solution governed by two arbitrary constants. For later convenience we label these  $\alpha$  and  $\gamma$ , where

$$\alpha = \frac{\Omega_m^2 \Omega_\Lambda}{(\Omega_m + \Omega_r + \Omega_\Lambda - 1)^3} = \frac{(8\pi G \rho_m R^3)^2 \Lambda}{27}, \quad (13)$$

and

$$\gamma = \frac{\Omega_r \Omega_\Lambda}{(\Omega_m + \Omega_r + \Omega_\Lambda - 1)^2} = \frac{8\pi G \rho_r R^4 \Lambda}{9}. \quad (14)$$

Present knowledge of  $\Omega_m$ ,  $\Omega_r$  and  $\Omega_\Lambda$  fixes  $\alpha$  and  $\gamma$ , and so picks out a unique curve. The curve will be valid back to last scattering, beyond which the equation of state becomes more complicated.

The diagrams in figure 1 highlight the fact that as the universe evolves the flow lines refocus around the spatially flat case,  $\Omega_M + \Omega_\Lambda = 1$ . One can argue that ‘most’ models concentrate around spatial flatness, though a more precise statement of this observation requires a more detailed model of how the initial conditions are set up. What is clear is that, for a large range of initial conditions, by the time we reach the current value of  $\Omega_M \approx 0.3$  most models are not far off spatial flatness. This prediction contrasts with models without a cosmological constant, where any slight deviation from the critical density in the early universe is scaled enormously by the time we reach the present epoch, implying that the parameters in the early universe are highly fine-tuned. One can see the problem straightforwardly by writing

$$\kappa = \Omega_m + \Omega_r + \Omega_\Lambda - 1. \quad (15)$$

The parameter  $\kappa$  measures the deviation from spatial flatness, and satisfies

$$\frac{\dot{\kappa}}{\kappa} = H(\Omega_m + 2\Omega_r - 2\Omega_\Lambda). \quad (16)$$

If  $\Omega_\Lambda = 0$  the right-hand side is always positive, and nothing prevents the continued growth of  $\kappa$ . The presence of a  $\Lambda$  term changes this completely. At some finite time  $2\Omega_\Lambda$  will overtake the matter terms, and  $\kappa$  is refocused back to  $\kappa = 0$ . So in this sense it can be argued that the presence of a cosmological constant can solve the flatness problem. The weakness with this picture is that one still has to explain why  $\Lambda$  takes on the value it does, which would appear to require fine tuning of its own. We now turn to a possible solution to this problem.

### 3 De Sitter Space and a Preferred $\Lambda$ Model

The considerations in the previous section apply solely to the existence of a cosmological constant, and do not imply any preference for spatially closed, flat or open universes. Of course, there are many theoretical reasons for preferring spatial flatness. These include the difficulties in constructing a homogeneous stress-energy tensor for Dirac fermions in anything other than a spatially-flat universe [10, 11]. But from a geometric perspective, the existence of a  $\Lambda$  term points us firmly in the direction of de Sitter space as a suitable background. In the absence of any firm evidence for a varying cosmological constant, this is the geometry to which we now turn.

The geometry of de Sitter space has a number of remarkable features. It is a space of constant negative curvature, forming the Lorentzian analogue of the non-Euclidean geometry discovered by Lobachevskii and Bolyai [2, 3]. Two-dimensional non-Euclidean geometry has an elegant construction in terms of the Poincaré disc, in which geodesics are represented as ‘ $d$ -lines’ — circles that intersect the disc boundary at right-angles (see figure 2). We can provide a similar picture for 2-dimensional de Sitter space, which is sufficient to capture the key features of the geometry. We start with an embedding picture, representing

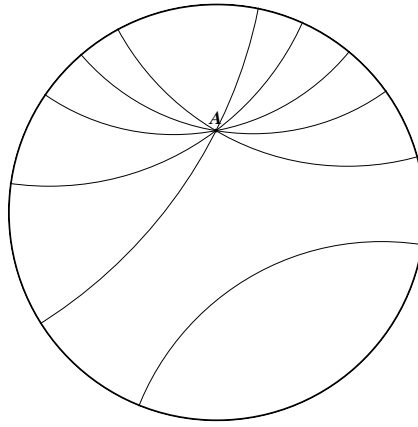


Figure 2: *The Poincaré disc.* Points inside the disc represent points in a 2-dimensional non-Euclidean (hyperbolic) space. A set of  $d$ -lines are also shown. These are (Euclidean) circles that intersect the unit circle at right angles. Given a  $d$ -line and point  $A$  not on the line, one can find an infinite number of lines through  $A$  that do not intersect the line.

de Sitter space as the 2-surface defined by

$$T^2 - X^2 - Y^2 = -a^2, \quad (17)$$

where  $(T, X, Y)$  denote coordinates in a space of signature  $(1, 2)$  and  $a$  is a constant. The resulting surface is illustrated in figure 3. The figure illustrates a key property of the entire de Sitter geometry, which is that spatial sections are closed, whereas the timelike direction is open. So de Sitter space describes a closed universe that lasts for infinite time. (One can set up local coordinate patches for which spatial sections are flat or open, but these coordinates are not global.) Null geodesics are straight lines formed by the intersection of the surface and a vertical plane a distance  $a$  from the timelike axis. Despite the fact that the space is spatially closed, the furthest a photon can travel is half of the way round the universe.

To establish an analogous picture to the Poincaré disc for de Sitter space, we start by considering the spatial section at  $T = 0$ . This section is a ring of radius  $a$ , which is mapped onto a straight line in a  $(1, 1)$  Lorentzian space via a stereographic projection. Null geodesics from this section are now represented as  $45^\circ$  straight lines in Lorentzian space. Since geodesics from opposite points on the ring meet at infinity, we arrive at a boundary in the timelike direction defined by a hyperbola. This construction provides us with a Lorentzian view of de Sitter geometry. Timelike geodesics in de Sitter space are represented by hyperbolae that intersect the boundary at a right-angle (see figure 4). Here ‘right-angle’ is defined in its Lorentzian sense (the tangent vectors have vanishing Lorentzian inner product). This view has the convenient feature that geodesics are lines of constant Lorentzian distance from some fixed point. The metric

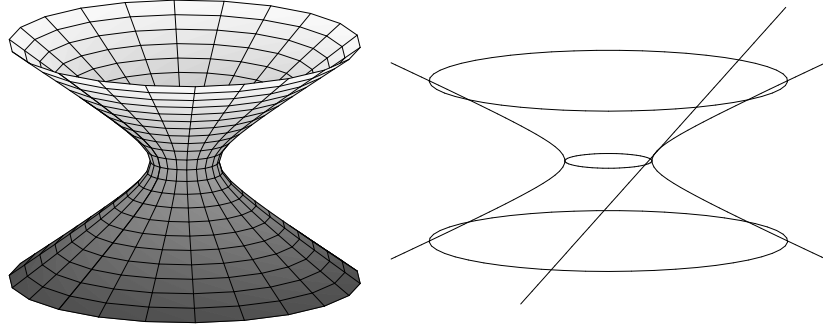


Figure 3: *Two-dimensional de Sitter Space.* The timelike direction is vertical, and spatial sections are closed. The right-hand diagram shows a null geodesic, which is a straight line in the embedding space.

associated with this view of de Sitter geometry has the conformal structure

$$ds^2 = \frac{a^4}{(a^2 + x^2 - t^2)^2} (dt^2 - dx^2), \quad (18)$$

which makes it clear that null geodesics must remain as straight lines in the  $x$ - $t$  plane.

There are many fascinating geometrical structures associated with de Sitter geometry, many of which mirror those of non-Euclidean geometry. For example, one can always find a reflection that takes any point to the origin [4]. One can then prove a number of results at the origin (where the geodesics are all straight lines) and the results are guaranteed to hold at all points. Much effort has gone into constructing quantum field theories in de Sitter space [12, 13, 14, 15]. There are two reasons why this is more complicated than in Minkowski space. The first is that spatial sections are closed, giving rise to a quantization condition. The second is the presence of event horizons, which gives rise to ambiguities in the definition of the vacuum.

Suppose now that we seek to describe the final fate of the universe faithfully within a de Sitter geometry. An immediate conclusion is that the universe has to be spatially closed, even though it expands for ever. Furthermore, since all cosmological models are conformally flat, it must be possible to represent the entire history of the universe within a diagram of the form of figure 4, with future infinity represented by the hyperbolic boundary. The big bang is then represented by a surface at some finite time in the conformal diagram. But now we begin to see a natural boundary condition emerging. Suppose that we insist that  $t = 0$  represents the initial singularity, so that the entire history of the universe can be conformally mapped into the top half of the de Sitter diagram. (This does not imply that the actual universe is static, it is merely a statement about its conformal representation.) This condition implies that any photon emitted at  $t = 0$  must travel precisely one-quarter of the way round the universe in the entire future evolution of the universe. An alternative way of saying this is that the past horizon projected back to  $t = 0$  should cover half of the de Sitter geometry.

Given an equatorial angle  $\phi$  on a 3-sphere, a photon travelling round the

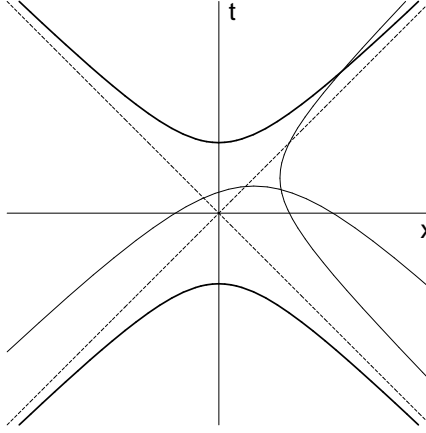


Figure 4: *The Lorentzian view of two-dimensional de Sitter space.* The boundary is defined by two hyperbolae (shown with thick lines). All geodesics through the origin are straight lines, and null geodesics are always straight lines at  $45^\circ$ . Two further geodesics, one spacelike and one timelike, are also shown. These are hyperbolae which do not pass through the origin. The timelike geodesic intersects the boundary in such a way that the two tangent vectors have vanishing Lorentzian inner product.

equator will satisfy

$$\frac{d\phi}{dt} = \frac{1}{R}, \quad (19)$$

where  $t$  is cosmic time. Traversing the entire universe corresponds to running from  $0 \leq \phi \leq 2\pi$ . If a photon is only to travel one-quarter of the way round we therefore require that

$$\int_0^\infty \frac{dt}{R} = \int_0^\infty \frac{dR}{R(-1 + \Lambda R^2/3 + 8\pi\rho R^2/3)^{1/2}} = \pi/2. \quad (20)$$

At this point is is useful to define the conformal time  $\eta$  by

$$\eta = \int_0^t \frac{dt'}{R(t')}. \quad (21)$$

The boundary condition then states that the end of the universe corresponds to a total passing of  $\pi/2$  units of conformal time.

For the case of a universe filled with non-interacting dust and radiation we can write equation (20) as

$$\int_0^\infty \frac{dx}{(\beta x^4 + x^3 - x^2 + \alpha)^{1/2}} = \pi/2, \quad (22)$$

where

$$\beta = \frac{\gamma}{\alpha} \quad (23)$$

with  $\alpha$  and  $\gamma$  as defined by equations (13) and (14) respectively. Equation (22) therefore represents an eigenvalue problem for the dimensionless ratios  $\alpha$  and  $\beta$ .

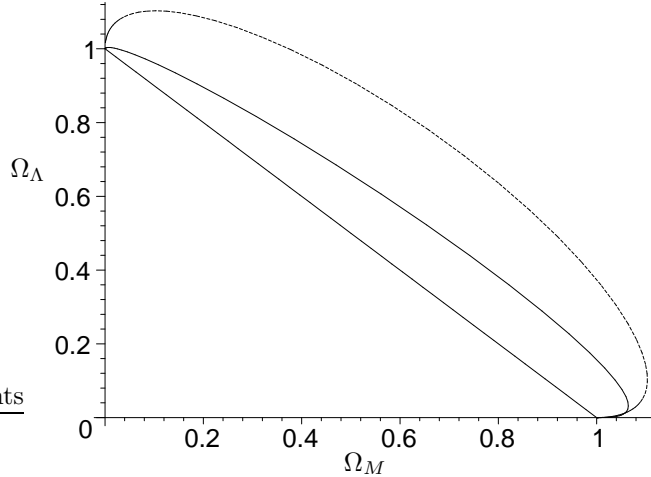


Figure 5: *Critical paths as predicted by the de Sitter embedding.* The solid line represents a matter-dominated universe, and the broken line shows radiation, for comparison. The straight line is the critical case of spatial flatness. By the time we reach  $\Omega_M \approx 0.3$  the universe has been driven close to critical density.

For the case of dust ( $\beta = 0$ ) the solution turns out to be  $\alpha \approx 40.468$ . Pinning down a value of  $\alpha$  and  $\beta$  picks out a unique trajectory in the  $\Omega_M$ – $\Omega_\Lambda$  plane. For example, for a dust cosmology we can use the value of  $\alpha$  to seed the flow-line around  $t = 0$ , since in this case  $\alpha$  is precisely the parameter  $A$  of equation (10). For the straightforward cases of dust ( $\beta = 0$ ) and radiation ( $\alpha = 0$ ) we arrive at the two curves shown in figure 5. As the universe is expected to be matter dominated for most of its history, the solid line in figure 5 is the more physically-relevant. Taking the present-day energy density to be around  $\Omega_M = 0.3$ , we see that  $\Omega_\Lambda$  is predicted to be around  $\Omega_\Lambda \approx 0.83$ . That is, a universe that is closed at around the 10% ratio. Such a prediction is reasonably close to the observed value, though it is ruled out by the most recent experiments [1]. In section 4 we show how this prediction is modified by an inflationary phase, driving us closer to the experimental values.

The boundary condition  $\eta(\infty) = \pi/2$  can be arrived at through an alternative route that works entirely within the conformal representation of cosmological models. By this we mean that the line element is written in the form

$$ds^2 = \frac{1}{f^2} (dt^2 - dx^2 - dy^2 - dz^2), \quad (24)$$

which is conformally equivalent to Minkowski space. The existence of such a representation is guaranteed by the fact that the Weyl tensor vanishes in all cosmological models. The precise form of  $f$  depends on the spatial topology. In

appendix A we show that the three cases reduce to

$$\begin{aligned}
f &= \frac{t}{R \sin(\eta)} = g \left( \frac{2\lambda t}{\lambda^2 + r^2 - t^2} \right) \frac{t}{\lambda} && \text{closed} \\
f &= \frac{2\lambda}{R} && \text{flat} \\
f &= \frac{t}{R \sinh(\eta)} = \bar{g} \left( \frac{2\lambda t}{\lambda^2 + t^2 - r^2} \right) \frac{t}{\lambda} && \text{open}
\end{aligned} \tag{25}$$

where  $r^2 = x^2 + y^2 + z^2$  and the forms of  $g$  and  $\bar{g}$  depends on the model for the matter content. A de Sitter space (centred on  $t = 0 = t$ ) has the conformal line element

$$ds^2 = \frac{12\lambda^2}{\Lambda(\lambda^2 + r^2 - t^2)} (dt^2 - dx^2 - dy^2 - dz^2). \tag{26}$$

So clearly the only solutions which have any chance of matching onto this final state are those for a closed universe. Furthermore, the function  $g$  must satisfy

$$\lim_{\chi \rightarrow \infty} g(\chi) = \left( \frac{\lambda^2 \Lambda}{3} \right)^{1/2} \frac{1}{\chi} \tag{27}$$

where

$$\chi = \frac{2\lambda t}{\lambda^2 + r^2 - t^2} = \tan(\eta). \tag{28}$$

But since

$$g = \frac{\lambda}{R \sin(\eta)} \tag{29}$$

we must then have  $R \cos(\eta)$  tending to a constant at large times. This is only possible if  $\eta$  tends to  $\pi/2$ , recovering our earlier boundary condition. This derivation is instructive in that it reveals how the constraint can be imposed as a straightforward boundary condition on a differential equation. In this case, the equation for  $g(\chi)$  is

$$\chi^2(1 + \chi^2) \left( \frac{dg}{d\chi} \right)^2 + \frac{d}{d\chi}(g^2 \chi) = \frac{8\pi G \lambda^2 \rho}{3} + \frac{\lambda^2 \Lambda}{3}. \tag{30}$$

The task then is to solve this equation subject to the boundary condition that  $g$  falls off as  $1/\chi$  for large  $\chi$ .

## 4 Scalar Fields and Inflation

So far we have obtained a suggestive boundary condition on cosmological models, which arises from the requirement that the universe tends towards a de Sitter geometry which is centred around the initial singularity. This condition gets us close to the observed values of the cosmological parameters, though not close enough to be consistent with experiment. We now turn to a discussion of how these conclusions are altered by an inflationary phase, concentrating on the simplest model of a quadratic potential. In this model the matter sector is initially described simply by a real massive scalar field. For suitable initial conditions this system shows inflationary behaviour. These initial conditions

are usually set at the start of the inflationary period, where the conditions are viewed as arising from some quantum fluctuation. But to apply our boundary condition we need to track the equations right back to the initial singularity, so that we can correctly locate the initial point. This turns out to require a power series in  $\ln(t)$ . Inflation on its own does not eliminate singularities from cosmology [16], so here we adopt a fairly traditional approach and examine the evolution of the matter density as it exits the big bang.

The Lagrangian density for the real scalar field  $\phi$ , with all dimensional constants included, is given by

$$\mathcal{L} = \frac{\hbar c}{2} \left( g^{\mu\nu} \partial_\mu \phi \partial_\nu \phi - \frac{m^2 c^2}{\hbar^2} \phi^2 \right). \quad (31)$$

Here  $\phi$  has dimensions of  $(\text{length})^{-1}$ , which is the convention widely adopted in the cosmology literature (though this does differ from the relativistic quantum mechanics literature [17]). The cosmological equations are most simply written as

$$\dot{H} + H^2 - \frac{c^2 \Lambda}{3} + \frac{4\pi G \hbar}{3c} \left( \frac{2\dot{\phi}^2}{c^2} - \frac{m^2 c^2}{\hbar^2} \phi^2 \right) = 0 \quad (32)$$

and

$$\ddot{\phi} + 3H\dot{\phi} + \frac{m^2 c^4}{\hbar^2} \phi = 0. \quad (33)$$

As we are only interested in closed universe models, the scale factor is given explicitly by

$$\frac{1}{R^2} = \frac{4\pi G \hbar}{3c^3} \left( \frac{\dot{\phi}^2}{c^2} + \frac{m^2 c^2}{\hbar^2} \phi^2 \right) - \frac{H^2}{c^2} + \frac{\Lambda}{3}. \quad (34)$$

For numerical work, and to help construct a series expansion around the singularity, it is useful to convert all of the equations into dimensionless form. There are two ways to do this, depending on whether one scales using the particle mass or the Planck mass. Both are useful in practice for numerical work, and the simple scaling argument described below can be used to convert between them. Here we convert to dimensionless form by employing the Planck mass  $m_p$ , time  $t_p$  and distance  $l_p$ . We define the dimensionless quantities

$$u = \frac{t}{t_p}, \quad \mu = \frac{m}{m_p}, \quad (35)$$

and henceforth  $\phi$ ,  $H$  and  $\Lambda$  are assumed measured in units of  $l_p^{-1}$ ,  $t_p^{-1}$  and  $l_p^{-2}$  respectively. In dimensionless terms the equations become

$$\frac{dH}{du} + H^2 - \frac{\Lambda}{3} + \frac{4\pi}{3} \left( 2 \left( \frac{d\phi}{du} \right)^2 - \mu^2 \phi^2 \right) = 0 \quad (36)$$

and

$$\frac{d^2\phi}{du^2} + 3H \frac{d\phi}{du} + \mu^2 \phi = 0. \quad (37)$$

Given a solution to this pair of equations, a new solution set is generated by scaling with a constant  $\sigma$  and defining

$$H'(u) = \sigma H(\sigma u), \quad \phi'(u) = \phi(\sigma u), \quad \mu' = \sigma \mu, \quad \Lambda' = \sigma^2 \Lambda. \quad (38)$$

This scaling property has a number of useful features. For example, if the desired value for  $\mu$  is small, we can scale to a numerically convenient value, integrate forwards in time, and then rescale the result at the end. Furthermore, many physically interesting quantities turn out to be invariant under changes in scale. These include the conformal time  $\eta$ , which is easily confirmed to be scale invariant from equation (21). Invariant quantities such as  $\eta$  turn out to be extremely helpful when considering the initial conditions as the universe emerges from the big bang. The scaling property does not survive quantisation, however, so has to be employed carefully when considering vacuum fluctuations.

As the universe emerges from the big bang the dominant behaviour of  $H$  is to go as  $1/(3t)$ . Equation (36) then implies that  $\phi$  must contain a term going as  $\ln(t)$ . But this in turn implies that  $H$  must also contain a term in  $t \ln(t)$ , in order to satisfy equation (37). Working in this manner we conclude that a series expansion in terms of  $\ln(t)$  is required to describe the behaviour around the singularity. We therefore write

$$H(u) = \sum_{i=0}^{\infty} H_i(u) \ln^i(u) \quad (39)$$

$$\phi(u) = \sum_{i=0}^{\infty} \phi_i(u) \ln^i(u). \quad (40)$$

Substituting these into the two equations, and setting each coefficient of  $\ln(u)$  to zero, we establish that

$$\begin{aligned} H_1 = & -u \frac{dH_0}{du} - u H_0^2 + \frac{u\Lambda}{3} - \frac{8\pi u}{3} \left( \frac{d\phi_0}{du} \right)^2 - \frac{16\pi\phi_1}{3} \frac{d\phi_0}{du} \\ & - \frac{8\pi\phi_1^2}{3u} + \frac{4\pi\mu^2 u\phi_0^2}{3}, \end{aligned} \quad (41)$$

with further algebraic equations holding for  $H_2, \phi_2, H_3, \phi_3$ , and so on. So by specifying  $H_0$ ,  $\phi_0$  and  $\phi_1$ , all the remaining terms in the solution are fixed. The aim then is to choose the three input functions to ensure that successive terms in the series get progressively smaller. This turns out to provide just the right number of equations to specify all coefficients, save for two arbitrary coefficients in  $\phi_0$ . The end result is a series controlled entirely by a pair of arbitrary constants: the expected number of degrees of freedom once we have fixed the singularity to  $t = 0$ . In order to generate curvature it turns out that the input functions need to be power series in  $u^{1/3}$ , which ensures that the scale factor goes as  $u^{1/3}$  at small times. The series solution is only required to find suitable initial conditions for numerical evolution, so only the first few terms are required. Expanding up to order  $u^{5/3}$  we find that

$$\begin{aligned} H_0 = & \frac{1}{3u} + \frac{32\sqrt{3\pi}}{27} b_4 u^{1/3} \\ & + \left( \frac{2\mu^2}{81} + \frac{\Lambda}{3} + \frac{4\pi}{3} \mu^2 b_0^2 + \frac{4\sqrt{3\pi}}{27} \mu^2 b_0 \right) u - \frac{6656\pi b_4^2}{891} u^{5/3}, \end{aligned} \quad (42)$$

$$\begin{aligned} \phi_0 = & b_0 + b_4 u^{4/3} - \frac{118\sqrt{3\pi} b_4^2}{99} u^{8/3} \\ & - \frac{1}{1296\pi} \left( 11\sqrt{3\pi} \mu^2 - 54\sqrt{3\pi} \Lambda - 216\sqrt{3} \pi^{3/2} \mu^2 b_0^2 + 36\pi\mu^2 b_0 \right) u^2 \end{aligned} \quad (43)$$

and

$$\phi_1 = -\sqrt{\frac{1}{12\pi}} - \frac{\mu^2}{216\pi} \left( -\sqrt{3\pi} + 36\pi b_0 \right) u^2. \quad (44)$$

Under scaling we find that the three key parameters in the model transform as

$$\mu \mapsto \sigma\mu, \quad b_0 \mapsto b_0, \quad b_4 \mapsto \sigma^{4/3}b_4. \quad (45)$$

The scaling transformation for  $b_4$  is entirely as expected, given that it is the coefficient of  $u^{4/3}$  in the series for  $\phi_0$ . We could have written our series in terms of  $(\mu u)$  to ensure the coefficients are all scale invariant, but the present scheme works well in practice.

The fact that  $b_4$  controls the curvature can be seen from equation (34) which, to leading order, yields

$$\frac{R}{l_p} = \left( \frac{2187}{12544\pi} \right)^{1/4} \frac{u^{1/3}}{\sqrt{-b_4}} + \dots \quad (46)$$

Clearly, the arbitrary constant  $b_4$  must be negative for a closed universe. As the universe is described by a 3-sphere of radius  $R$ , the total volume of the universe is given to leading order by

$$V = 2\pi^2 \left( \frac{2187}{12544\pi} \right)^{3/4} \frac{l_p^3}{(-b_4)^{3/2}} u + \dots \quad (47)$$

One interesting calculation we can perform in a closed universe is to find the total energy contained within it. By integrating the energy density we find that

$$E_{\text{tot}} = \frac{\pi}{12} \left( \frac{2187}{12544\pi} \right)^{3/4} \frac{1}{(-b_4)^{3/2}} \frac{\hbar}{t} + \dots \approx 0.03 \left( \frac{-\mu^{4/3}}{b_4} \right)^{3/2} \frac{\hbar}{\mu^2 t}. \quad (48)$$

We return to a discussion of this equation in section 7.

The plot in figure 6 illustrates the general behaviour of these cosmologies. As the universe emerges from the big bang the energy density in the scalar field is dominated by the  $\dot{\phi}$  term, and the field behaves as if it is massless. It follows that  $H$  initially goes as  $1/(3t)$ . But once  $H$  has fallen sufficiently far we enter a region in which  $m^2\phi^2$  starts to dominate over  $\dot{\phi}^2$ . These are suitable initial conditions for the universe to enter an inflationary phase. By varying  $b_0$ ,  $b_4$  and  $\mu$  we control both the values of the fields as we enter the inflationary period, and how long the inflationary period lasts. The cosmological constant plays no significant role in this part of the evolution. The dynamics displayed in this figure is quite robust over a wide range of input parameters.

The typical behaviour as we exit the inflationary region is shown in figure 7. The end of inflation is characterised by  $H \approx \mu$ . Beyond this point the scalar field enters an oscillatory phase, with the time-averaged fields satisfying the conditions for a simple matter-dominated cosmology. In this case the  $H$  function can be approximated by a curve going as  $2/3(t - t_0)$ , describing a dust model with a displaced origin. The universe then appears as if it has been generated by a big bang at a later time. We call this the effective big bang. Of course, around this time we expect reheating effects to start to dominate, so that in reality the universe must pass over to a radiation-dominated era. However,

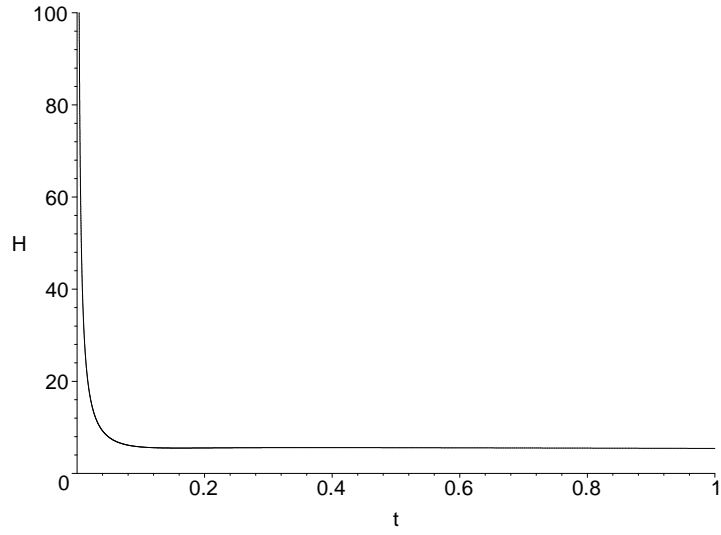


Figure 6: *Hubble function entry into the inflationary regime.* The Hubble function emerges from the big bang going as  $1/3t$ . As  $H$  falls it quickly enters the inflationary region, during which it falls linearly. Time  $t$  is measure in units of  $t_p$ , and  $H$  in units of  $t_p^{-1}$ . The input parameters were set to  $b_0 = 2.48$ ,  $b_4 = -0.51$  and  $m = m_p$ . The cosmological constant term has no effect in this region and can be set to zero.

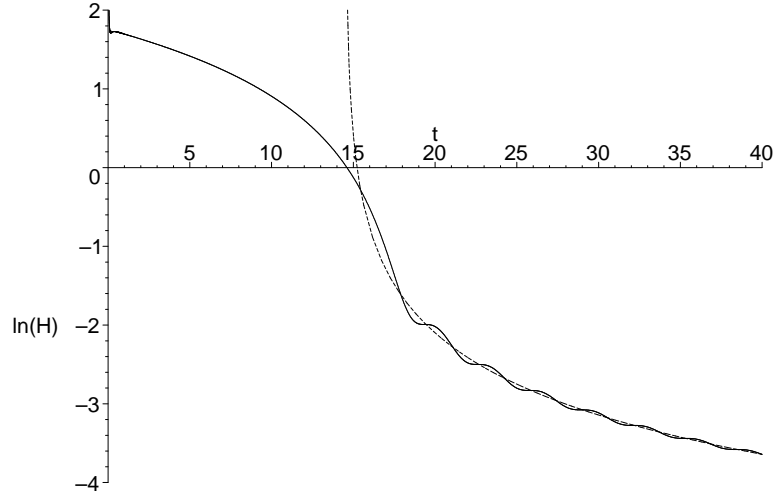


Figure 7: *Hubble function exit from the inflationary regime.* As the inflationary era ends the density and pressure start oscillating around values for a matter-dominated cosmology. The effective singularity for this dust cosmology is displaced from  $t = 0$ . The broken line plots the natural log of  $2/3(t - 14.56)$ . The parameters in this model are  $b_0 = 2.48$ ,  $b_4 = -0.51$  and  $m = m_p$ .

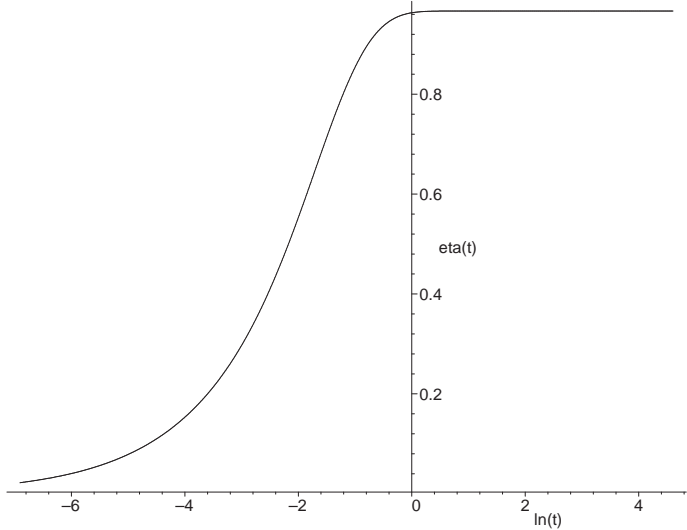


Figure 8: *Evolution of the conformal time  $\eta(t)$  as a function of  $\ln(t)$ .* The parameters for the model are as given in figure 7 and again  $t$  is measured in units of the Planck time.

the naive ‘effective big bang’ concept is useful for extracting some qualitative predictions from our model.

As well as giving a new effective start time for the big bang, inflation must also resolve the horizon problem. The conformal picture provides a straightforward means of visualising this process. The key is to compute how much conformal time has elapsed by the end of the inflationary era. Using the same parameters as in figure 7 we find that the conformal time evolves as shown in figure 8. As the universe emerges from the (real) big bang  $\eta$  initially grows at  $t^{2/3}$ , as can be seen from equation (46). This gives rise to the rapid growth seen in figure 8, which plots  $\eta$  as a function of  $\ln(t/t_p)$ . But once the inflationary region is entered,  $R(t)$  starts to increase rapidly. So the conformal time, which involves the time integral of  $R^{-1}$ , quickly saturates, as can also be seen in figure 8. Any further increase in  $\eta$  will take an extremely long time to occur, since the integrand  $1/R$  is extremely small. So if  $\eta$  has not reached  $\pi/2$  before  $R$  has inflated significantly, the universe will have to exist for an extremely long time to reach the boundary value of  $\pi/2$ .

This growth in  $\eta$  is important for resolving the horizon problem. For the parameters used in figures 7 and 8 we see that  $\eta$  saturates at a value of around 0.97 by the end of inflation (at around  $t = 100t_p$ ). The value of  $R$  at this time is  $2 \times 10^{22}l_p$ . (This is still quite a small value of  $R$ , which is a consequence of the large mass chosen here.) All changes in  $\eta$  beyond the end of inflation occur very slowly. Irrespective of the properties of the reheating phase,  $\eta$  will have changed very little by the time recombination occurs. This pushes the era of recombination to a much later conformal time, close to the value for the present epoch. This removes the horizon problem, as the observable patch of the universe has been in causal contact and has had sufficient time to thermalise (see figure 9). This is not true of the universe as a whole, as antipodal points

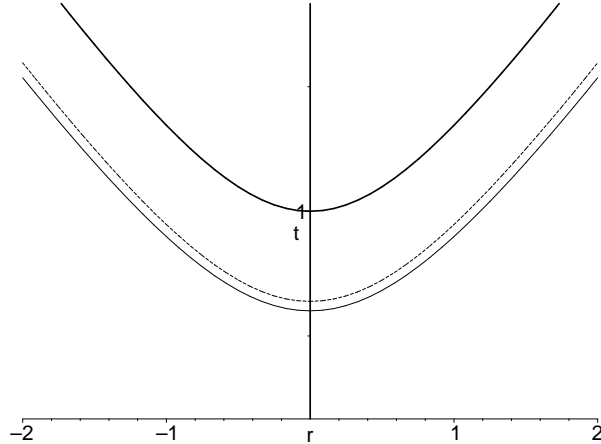


Figure 9: *The horizon problem for a closed universe in the conformal picture.* The lower solid line represents the surface of last scattering, and the broken line just above it is the current epoch. The thick line is the future boundary ( $t = \infty$ ). Null geodesics lie at  $45^\circ$ , so there is no problem with points in the observable part of the surface of last scattering having once been in causal contact.

remain outside each other's light cone until  $t = \infty$ .

In order to make some initial crude estimates from our boundary condition, we will ignore the effects of reheating and nucleosynthesis, and assume that the universe just smoothly enters a matter-dominated phase described by

$$R = R_1 \left( \frac{t - t_0}{t_1 - t_0} \right)^{2/3}. \quad (49)$$

For the parameters we are currently considering we have  $R_1 = 2 \times 10^{22} l_p$ ,  $t_0 = 14.56 t_p$  and  $t_1 = 100 t_p$ . We will also ignore the cosmological constant, though this will clearly affect the behaviour at late times. The conformal time elapsed at some later cosmic time  $t$  can be approximated by

$$\eta \approx \eta(t_1) + \frac{3}{R_1} (t - t_0)^{1/3} (t_1 - t_0)^{2/3} \approx 0.97 + 2.4 \times 10^{-19} t^{1/3}, \quad (50)$$

where  $t$  is measured in units of the Planck time. We can therefore arrive at a crude estimate for the age of the universe simply by setting  $\eta = \pi/2$ . This gives a time of  $1.6 \times 10^{61}$  in Planck units, or about  $2.8 \times 10^{10}$  years. This is a good illustration of how some very large numbers (such as the age of the universe in Planck times) can emerge from a simple model of inflation, augmented with our closed universe boundary condition.

In order to produce a more detailed prediction, we return to considering trajectories in the  $\Omega_M - \Omega_\Lambda$  plane. We can still assume that the universe is essentially matter dominated throughout its history, but now the total amount of conformal time that should elapse along the trajectory is less than  $\pi/2$ . The effect of this is to drive us onto trajectories which are closer to the critical line. This is clear from equation (22), with  $\beta = 0$ , as the value of the integral

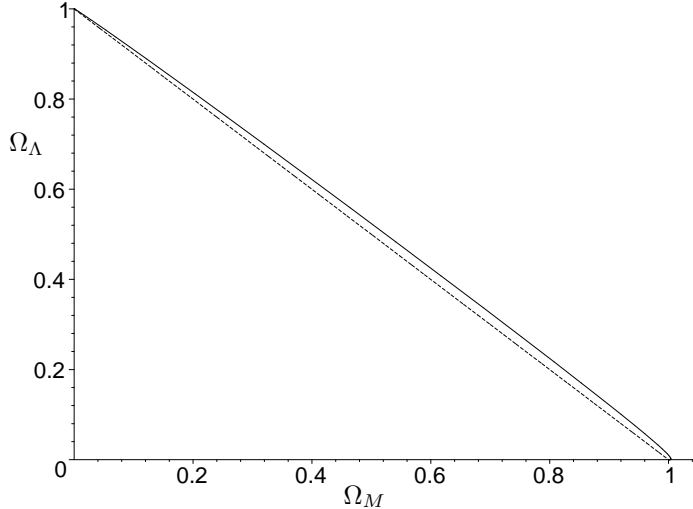


Figure 10: *Matter-dominated trajectory in the  $\Omega_M$ - $\Omega_\Lambda$  plane.* The trajectory (solid line) is picked out by demanding that the total conformal time elapsed throughout the evolution is 0.6. This evolution joins onto an inflationary model which takes up around 0.97 units of conformal time, so that the boundary condition of a total of  $\pi/2$  is obeyed.

decreases as we increase the parameter  $\alpha$ . This in turn steepens the gradient of the trajectory by increasing the parameter  $A = \alpha$  in equation (10). If we only require a total conformal time of around 0.6 to elapse during the matter-dominated phase of the universe (as for the model above), then we require an  $\alpha$  of around  $10^4$ , producing a trajectory which is very close to spatially flat, and predicting a universe which is currently closed at around the 1% level (see figure 10).

We can now see that our boundary condition gives rise to a remarkable seesaw mechanism, that has two key components. The first component relates to the amount of inflation that occurs. For a range of conditions, the time at which inflation starts can be approximated by

$$u_i = \frac{1}{(12\pi)^{1/2} \mu b_0}. \quad (51)$$

A check on the physical approximations we make here is that this quantity has the correct scale transformation properties under the transformation of equation (45). The value of  $H$  at the start of slow-roll inflation can be approximated by  $1/(3u_i)$ ,

$$H_i = \frac{1}{3u_i}, \quad (52)$$

and a suitable condition for the end of slow roll can be taken as

$$H_f^2 = \frac{\mu^2}{3}. \quad (53)$$

During slow roll the evolution of  $H$  is well approximated by a linear fit, so

$$H = H_i - \frac{u - u_i}{u_f - u_i} (H_i - H_f). \quad (54)$$

The gradient is determined from the field equations to be

$$\frac{H_i - H_f}{u_f - u_i} = \frac{\mu^2}{3}. \quad (55)$$

The total number of e-foldings,  $N$ , can therefore be approximated by

$$N = \int_{u_i}^{u_f} H \, du \approx \frac{3}{2\mu^2} (H_i^2 - H_f^2) \approx 2\pi b_0^2. \quad (56)$$

Numerical simulations reveal that this approximation does give a correct order-of-magnitude for the number of e-foldings, though it does tend to underestimate the precise value. As expected, the result for  $N$  is invariant under scale changes, as is clear from the integral formula for  $N$ . The key conclusion is that the number of e-foldings is primarily determined by  $b_0$ , with the value of  $H$  at the end of inflation fixed by  $\mu$ . The value of  $b_4$  essentially decouples from  $N$ . An increase in  $b_0$  leads to an increase in the final value of  $R$ , and hence to an increase in  $\rho R^3$  in the matter phase. From equation (13) we see that, in order to preserve  $\alpha$ , any increase in  $\rho R^3$  must be offset by a decrease in the cosmological constant. Conversely, the observed value of  $\Lambda$  can be employed to constrain the amount of inflation.

The second quantity of interest, given our boundary condition, is the amount of conformal time that has elapsed before the universe enters the present matter-dominated epoch. Figure 8 shows the typical evolution of  $\eta$ . We see that a large percentage of the conformal time is taken up before inflation starts. During this region we can approximate  $R$  by equation (46). Taking  $u_i$  as roughly approximating the point where  $\eta$  starts to saturate, we find that the conformal time evolved is approximated by

$$\eta = \int_0^{u_i t_p} \frac{dt}{R} \approx 0.92 \left( \frac{|b_4|}{\mu^{4/3}} \right)^{1/2} \left( \frac{1}{b_0^2} \right). \quad (57)$$

And again, the result naturally assembles into a scale-invariant quantity. This result typically underestimates the total elapsed  $\eta$  at the end of inflation, but it does set a useful restriction on the order of magnitude of the expression on the right-hand side. We now see that, for fixed  $b_0$  and  $\mu$ , the greater the initial curvature (increasing  $|b_4|$ ), the greater the amount of conformal time taken up during inflation. This in turn forces the universe today to be closer to flat. And conversely, the more spatially curved we want the universe to be today, the closer to flat it must be initially. This is the second component of the seesaw mechanism. The observed values of the cosmological parameters, together with our boundary condition, therefore place a severe restriction on the allowed models.

Given the strong constraints our model places on trajectories in the  $\Omega_M - \Omega_\Lambda$  plane, the model must predict the small value of the cosmological constant. To see how small values of  $\Lambda$  naturally arise, we return to equation (13) and write

$$\Lambda = \frac{27\alpha}{(8\pi G \rho_m R^3)^2}. \quad (58)$$

In order to make some useful approximations we will again ignore the effects of reheating and radiation domination, and simply assume that  $\rho_m R^3$  is given by

its value for the scalar field at the end of inflation. If we furthermore ignore the effects of curvature and  $\Lambda$ , we can write  $8\pi G\rho_m = 3H^2$ , so we have

$$\Lambda = \frac{3\alpha}{H^4 R^6} \Big|_{\text{end}}. \quad (59)$$

This expression does not depend on the precise moment of evaluation. As we have seen, typical values of  $\alpha$  are in the range  $10^3$  to  $10^5$ . The small value of  $\Lambda$  is therefore a consequence of the large values of  $RH^{2/3}$  achieved by the end of inflation. The value of  $H$  at the end of inflation is given by equation (53), and for  $R$  at the end of inflation,  $R_f$ , we can write

$$R_f = e^N R_i. \quad (60)$$

Here  $R_i$  is the value of  $R$  at the start of inflation, and  $N$  is the number of e-foldings. We can estimate  $R_i$  using equation (46) and the value of  $u_i$  from equation (51). Putting these together, we arrive at the approximate formula

$$\Lambda \approx 8 \times 10^4 \alpha \frac{|b_4|}{\mu^{4/3}} b_0^2 \mu^2 e^{-6N} l_p^{-2}. \quad (61)$$

The typical models we consider have  $N$  in the range of 40 to 50, and  $\mu$  around  $10^{-6}$ , which does indeed predict an extremely small value for the cosmological constant.

In summary, our model makes a series of predictions. Given only the observed values of  $H_0$ ,  $\Omega_M$  and  $\Omega_\Lambda$  we are forced to values of the scale-invariant parameters  $b_0$  and  $b_4/\mu^{4/3}$  both of order unity. Because we start in a big bang phase, with infinite  $H$ , the model *predicts* a period of inflation in the early universe, independent of any question of generating super-horizon fluctuations. Furthermore, our boundary condition ensures that the matter-dominated plot in figure 5 represents the *largest* departure from flat that we can consider. The inflationary period drives us closer to flat and, assuming  $\Omega_M \approx 0.3$  we are led to an  $\Omega_\Lambda$  of around 0.7. Viewed in reverse, given input parameters  $b_0$  and  $b_4/\mu^{4/3}$  of order unity, together with our boundary condition, we predict an extremely small value for  $\Lambda$ , consistent with observation. The final parameter in the model is  $\mu$ , which is fixed by considering the growth of perturbations during the inflationary period.

## 5 The Curvature Spectrum

Our proposed boundary condition places a strong restriction on the class of allowed models. We must now see whether any of these models produce a perturbation spectrum consistent with the observed primordial fluctuations in the CMB. Due to the scale-invariant nature of the equations (under the transformation of equation (38)), the parameters that determine the key features of the inflationary period are the scale-invariant quantities  $b_0$  and  $b_4/\mu^{4/3}$ . Furthermore, the restriction that the total amount of conformal time available is  $\pi/2$  constrains the combination in equation (57) to be of order 1. This essentially restricts us to a one-parameter class of models.

The scale transformation we have utilised at various points is not conserved by quantisation, so vacuum fluctuations impose an absolute scale on the model.

The key quantity that determines the size of the perturbations is the mass ratio  $\mu = m/m_p$ . For models with a quadratic potential to generate perturbations consistent with observation we need to set  $\mu$  to be around  $10^{-6}$ . As explained above, this value is irrelevant for the evolution of the scalar field, but  $\mu$  does set the absolute size of the Hubble function, and so fixes the magnitude of perturbations.

In order to consider a concrete example, we adopt the following set of parameters:

$$b_0 = 2.37, \quad \frac{b_4}{\mu^{4/3}} = -0.49, \quad \mu = 2.1 \times 10^{-6}. \quad (62)$$

Evidently, little fine tuning has gone into choosing the two scale-invariant combinations, both of which are of order unity. Furthermore, the predictions we make here are quite robust under variations of these parameters. We are a long way removed from areas of parameter space where chaotic dynamics of the type considered by Cornish & Shellard [18] could prove significant.

In a closed universe model there are two scales of interest: the horizon size  $1/H$ , and the radius of the spatial sections  $R$ . The ratio of these defines the dimensionless quantity  $1/(RH)$ , which is related to the closure density by

$$\Omega - 1 = \frac{1}{(RH)^2}, \quad (63)$$

where the total  $\Omega$  is defined by

$$\Omega = \Omega_\Lambda + \Omega_M. \quad (64)$$

During inflation  $\Omega$  should *decrease*, as the universe is driven towards flatness. This effect can be seen for our chosen parameters in figure 11, which confirms that the universe is accelerating over the range  $e^{11} < t/t_p < e^{16}$ . The plot also shows that the radius is always greater than the horizon size, which is important when considering perturbation modes.

The evolution of the scale factor for our chosen parameters is shown in figure 12. During the inflationary region  $\ln(R)$  increases from about 14 to 60.0. This corresponds to a total number of e-foldings of 46, as expected given our choice of parameters. This is roughly the figure we expect for the number of e-foldings if the universe departs from flatness by an amount that is visible today [6]. In order to give rise to the observed fluctuation spectrum it is thought that around 40–50 e-foldings are required between the point where the present horizon scale leaves the horizon and the end of inflation [19]. For this to hold, we therefore require that the present horizon scale leaves the Hubble horizon soon after the onset of inflation.

Closed universe models have an advantage over flat models when discussing scales and perturbations, because equation (63) gives direct expression for  $R$  in terms of  $\Omega$  and  $H$ . To apply this, suppose that at the current epoch a given physical size occupies a fraction  $x$  of the Hubble horizon  $1/H_0$ . The corresponding physical scale is

$$d_0 = \frac{x}{H_0}, \quad 0 < x < 1. \quad (65)$$

For wave modes,  $d_0$  will be quantised in units of  $2\pi R_0/n$ , where  $n$  is an integer. We will ignore this quantisation effect here, as the number of modes available

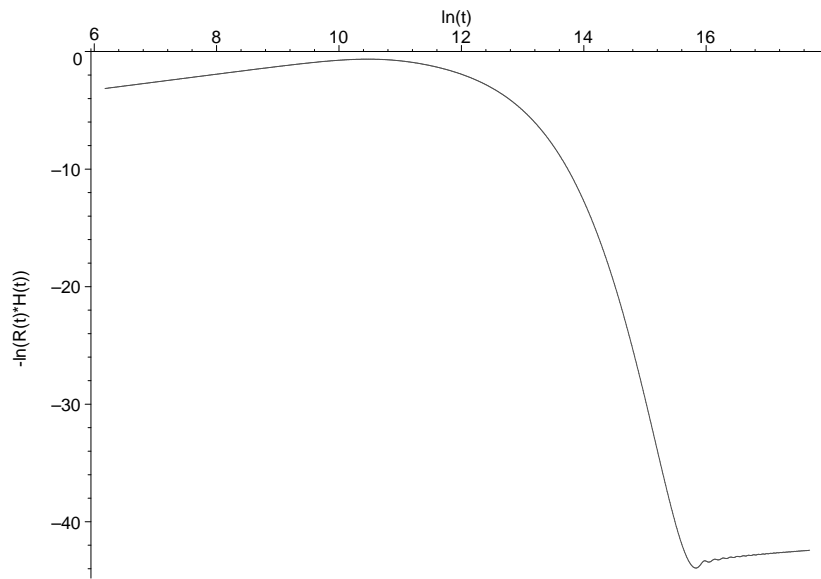


Figure 11: *Evolution of  $1/(RH)$* . The natural log of the dimensionless ratio of the Hubble radius to the curvature radius is plotted against log time (in units of  $t_p$ ). The parameters for the model are as described in the text. During the inflationary period,  $1/(RH)$  is a decreasing function of time, corresponding to an accelerating phase.

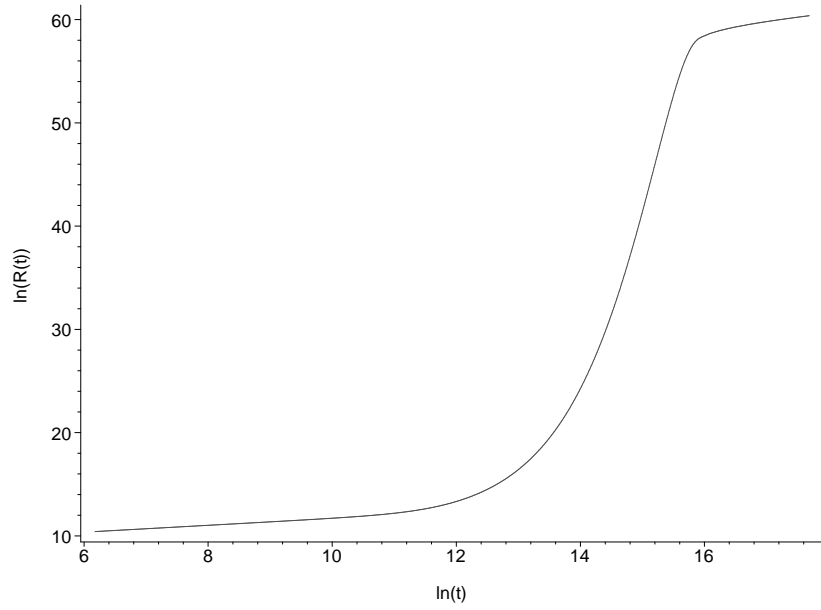


Figure 12: *Evolution of the scale factor*. The evolution of logarithm of the scale factor  $R/l_p$  is shown as a function of log time ( $t$  in units of  $t_p$ ).

ensure that a continuum is a reasonable approximation for all but the low- $k$  modes. Now consider the distance corresponding to  $d_0$  in an epoch when the scale factor is  $R$  instead of  $R_0$ . This scale is simply  $Rx/(R_0H_0)$ . This distance is equal to the Hubble horizon at the epoch corresponding to  $R$  when

$$\frac{Rx}{R_0H_0} = \frac{1}{H}. \quad (66)$$

(As is standard practice we formulate the conditions for horizon crossing in terms of the Hubble horizon, as opposed to the particle horizon.) It follows that the scale corresponding to a given  $x$  crosses the Hubble horizon when

$$x = \frac{R_0H_0}{RH} = \frac{\sqrt{\Omega - 1}}{\sqrt{\Omega_0 - 1}}. \quad (67)$$

So as  $\Omega$  is driven to unity during inflation, progressively smaller scales cross the horizon as time advances.

Figure 13 shows the behaviour of  $\Omega$  in our scalar field model. As expected,  $\Omega$  is driven close to 1 in the region  $e^{11} < t/t_p < e^{16}$ . In order to use this plot in conjunction with equation (67) we need to assign a value to  $\Omega_0$ . The most recent results from WMAP, with all data folded in, give a value of  $\Omega_0 = 1.02 \pm 0.02$  [1], so here we work with a value of  $\Omega_0 = 1.02$ . The scale corresponding to the present horizon size ( $x = 1$ ) is therefore obtained during inflation when  $\Omega = 1.02$ . Figure 13 shows that this occurs at  $\ln(t/t_p) = 12.0$ . By reference to figure 12, we see that this time corresponds to roughly 2 e-foldings. This leaves roughly 44 e-foldings to the end of inflation, which are sufficient to produce a fluctuation spectrum with the desired properties. These values are consistent with the estimates of Uzan, Kirchner & Ellis. [7].

Each value of  $x$  less than 1 corresponds to a scale which leaves the Hubble horizon at successively smaller values of  $\Omega$ . A remarkable feature of the approach outlined here is that it does not require any knowledge of the evolution of the universe to relate scales today to scales at the end of inflation. This is because in any closed (or non-flat) universe it is possible to measure  $R$  directly. This cannot be done if the universe is assumed to be flat throughout inflation, as one loses the ability to track scales through the evolution of  $\Omega$ . In flat models the only way to find the scale ratio  $R/R_0$  is to evolve the scale factor  $R$  through the history of the universe, including the epoch of reheating, about which little is known. Of course, our method would be impossible to apply if the value of  $\Omega_0$  turns out to be undetectably close to 1. This is predicted by approaches such as chaotic inflation, which can typically allow of order  $10^{10}$  e-foldings [19]. But for models that allow  $\Omega_0$  to deviate measurably from 1 the method we have outlined here should be of considerable use in calculating the fluctuation spectrum induced by inflation.

In order to compute the primordial curvature spectrum we adopt the slow-roll approximation, and closely follow the presentation of Liddle & Lyth [19]. For a quadratic potential, the slow roll condition can be expressed simply in terms of the single parameter  $\epsilon$ , where

$$\epsilon = \frac{1}{4\pi\phi^2}. \quad (68)$$

For slow roll to hold we require that  $\epsilon \ll 1$ . However, the model we consider here has  $\epsilon$  in the range from  $10^{-2}$  to  $10^{-1}$ , with the larger values corresponding to

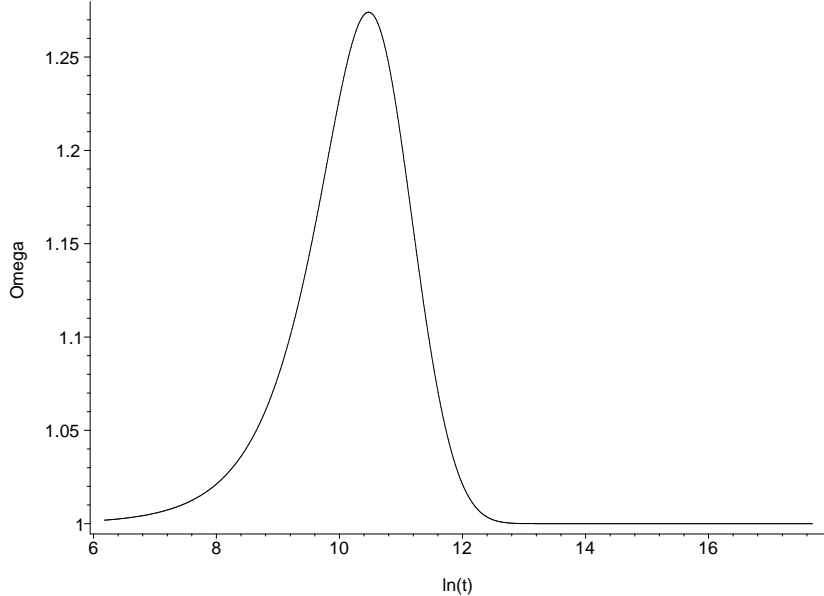


Figure 13: *Evolution of the total  $\Omega$  during inflation.* The total density is quickly driven close to flat, after which  $\Omega$  only changes slowly.

higher  $k$  values. We are therefore close to the point where slow roll ceases to be a good approximation. A concrete example of this is seen when we consider the spectral index (see also Martin & Schwarz [20] for a discussion of the precision of slow roll). For the main evolution of  $\phi$ , however, plots such as figure 6 confirm that the slow roll approximations are holding up, with the evolution of  $H$  roughly linear with the expected gradient of  $\mu^2/3$ . A further source of error, as stated earlier, is that we are ignoring the quantisation effects implied by a closed cosmology. This is only likely to have an effect at small  $k$  values, and if anything will imply that we overestimate the power in this region. Given these provisos, we still expect the simple, slow-roll equations do give a reasonably accurate prediction for the curvature spectrum.

Given the slow roll approximations, the key equation determining the curvature spectrum  $\mathcal{P}_{\mathcal{R}}(k)$  is [19]

$$\mathcal{P}_{\mathcal{R}}(k) = \left( \frac{H}{\dot{\phi}} \right)^2 \left( \frac{H}{2\pi} \right)^2, \quad (69)$$

where the right-hand side is evaluated when a given scale  $x$  crosses the horizon. If we write

$$\mathcal{P}_{\mathcal{R}}^{1/2}(k) = \frac{-H^2}{2\pi\dot{\phi}} \quad (70)$$

we see that the power spectrum is controlled by the ratio  $H^2/\dot{\phi}$ . This function is plotted in figure 14. Figures 13 and 14 contain all of the information required to extract  $\mathcal{P}_{\mathcal{R}}(k)$ . Given a comoving wavenumber  $k$ , we find  $x$  from

$$\frac{1}{k} = \frac{x}{H_0}. \quad (71)$$

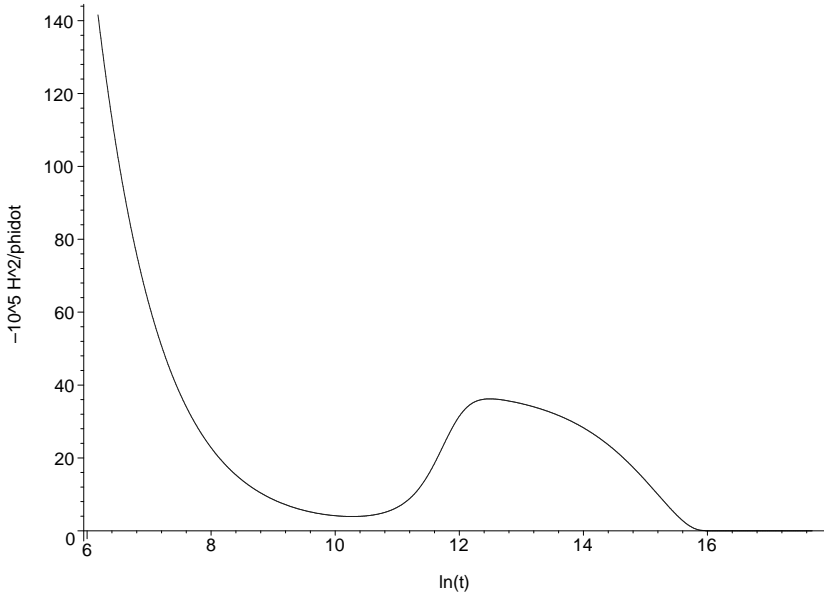


Figure 14: *Evolution of  $H^2/\dot{\phi}$  during inflation.* The function plotted is  $-10^5 H^2/\dot{\phi}$  as a function of  $\ln(t/t_p)$ . This function controls the magnitude of the curvature perturbation.

The value of  $x$  is converted to a time using equation (67) and the relationship plotted in figure 13. With the value of  $t$  then found, we can read off the spectrum from figure 14. The fact that the graph turns over for  $\ln(t/t_p) < 12$  suggests that the spectrum will contain less power at low- $k$  values than would be expected from a straightforward power law in a flat cosmology, in contrast to the predictions of Starobinsky [6].

It is convenient to plot perturbation spectra as a function of  $y = \ln(1/x)$ . With dimensions reinserted,  $y$  is given by

$$y = \ln \left( \frac{k}{h} \times 3 \times 10^3 \right) \quad (72)$$

where  $k$  is measured in  $\text{Mpc}^{-1}$  and the Hubble constant is given by  $H_0 = 100h \text{ km s}^{-1} \text{ Mpc}^{-1}$ . In figure 15 we plot the power spectrum as a function of  $y$  for our chosen parameters, including  $\Omega_0 = 1.02$ . (For a plot showing the power spectrum as an explicit function of  $k$  in  $\text{Mpc}^{-1}$  see figure 16.) The quantity plotted (solid curve) is  $10^{10}(2\pi)^2 \mathcal{P}_R(k)$ . The graph shows a clear cutoff at low- $k$  values. A cutoff of this type was proposed on phenomenological grounds by Efstathiou [21]. Indeed, it turns out that the type of exponential cutoff proposed by Efstathiou agrees remarkably well with our calculations, as can be seen in the dashed line, which plots

$$10^5 2\pi \mathcal{P}^{1/2}(k) = 37.6(1 - 0.023y)(1 - \exp(-(y + 0.93)/0.47)), \quad (73)$$

valid for  $y > -0.93$ . The fact that our model predicts a spectrum which has already been argued for on phenomenological grounds is very reassuring. We

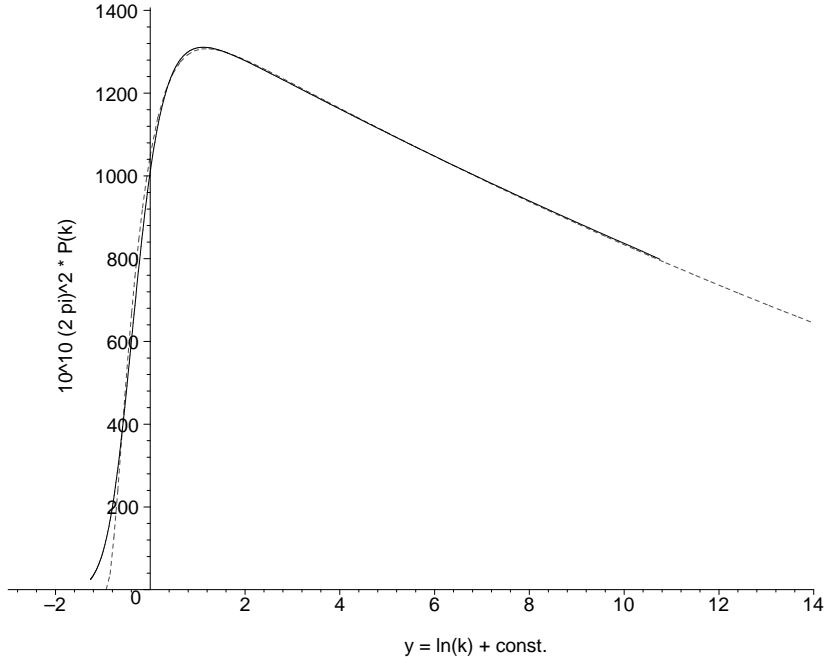


Figure 15: *The power spectrum of curvature perturbations.* The function plotted is  $10^{10}(2\pi)^2\mathcal{P}_R(k)$  as a function of  $y = \ln(1/x) = \ln(k) + \text{constant}$ . The solid line represents the numerical predictions from our model, and the broken line is the best-fit power law with an exponential cutoff. The parameters are described in the text.

can now see that our model will predict a deficit in the CMB power spectrum at low  $\ell$ , and in section 6 we confirm that this is the case.

Figure 15 contains a further surprise. From equation (73) we see that at large  $k$  the relationship between  $\mathcal{P}_R^{1/2}(k)$  and  $\ln(k)$  is roughly linear, which is quite different from the expected power law relation. To understand why this is the case we return to the slow roll equations and derive the form of the spectrum for a quadratic potential, following section 7.5 of Liddle and Lyth [19]. The main relation we require relates the derivatives with respect to  $k$  and  $\phi$ :

$$\frac{d}{d\ln k} = -\frac{1}{4\pi\phi} \frac{d}{d\phi}, \quad (74)$$

where we specialise to results for a quadratic potential. During slow roll the following approximate relations hold:

$$H^2 = \frac{4\pi}{3}\mu^2\phi^2, \quad \dot{\phi} = \frac{\mu}{\sqrt{12\pi}}. \quad (75)$$

It follows that the curvature spectrum is approximated by

$$\mathcal{P}_R^{1/2}(k) = 4\left(\frac{\pi}{3}\right)^{1/2} \mu\phi^2. \quad (76)$$

We therefore find that

$$\frac{d}{d \ln k} \mathcal{P}_{\mathcal{R}}^{1/2}(k) = -\frac{2\mu}{\sqrt{3\pi}}. \quad (77)$$

This confirms that the relationship between  $\mathcal{P}_{\mathcal{R}}^{1/2}(k)$  and  $\ln(k)$  is indeed linear. Furthermore, the gradient is predicted to be  $-2\mu/\sqrt{3\pi}$ . For the model we are considering this evaluates to  $1.35 \times 10^{-6}$ , which agrees well with the fit of equation (73), which has a gradient of  $37.6 \times 0.023/(2\pi \times 10^5) = 1.37 \times 10^{-6}$ . We can also see that

$$\frac{d}{d \ln k} \ln(\mathcal{P}_{\mathcal{R}}(k)) = -2 \frac{1}{\mathcal{P}_{\mathcal{R}}^{1/2}(k)} \frac{2\mu}{\sqrt{3\pi}} = -\frac{1}{\pi\phi^2} = -4\epsilon \quad (78)$$

where  $\epsilon$  is the slow-roll parameter of equation (68). The typical slow-roll approximation is to now write  $\mathcal{P}_{\mathcal{R}}(k) \propto k^{-4\epsilon}$ , so that

$$\mathcal{P}_{\mathcal{R}}^{1/2}(k) \approx Ak^{-2\epsilon} \approx A(1 - 2\epsilon \ln(k) + 2\epsilon^2 \ln^2(k) + \dots). \quad (79)$$

The higher order terms here are incorrect, and introduce an error of order  $\epsilon \ln(k)$  to the power spectrum. As commented earlier, at high- $k$  values  $\epsilon$  is in the range 0.01–0.1, so this deviation can become quite significant.

In figure 16 we compare our computed scalar power spectrum with the best fit power law ( $n_s = 0.96$ ) and the WMAP running spectral index best fit. The vertical normalisations for these fits have been chosen arbitrarily, since it is the shape of the spectrum at large  $k$  which is of greatest interest here. The WMAP running spectral index model shape is given by

$$\mathcal{P}_{\mathcal{R}}(k) = \mathcal{P}_{\mathcal{R}}(k_0) \exp \left( (n_s - 1) \ln(k/k_0) + \frac{1}{2} n_{\text{run}} (\ln(k/k_0))^2 \right). \quad (80)$$

Using the WMAP figures for combined data sets their best fit values are  $n_s = 0.93$ ,  $n_{\text{run}} = -0.031$  and  $k_0 = 0.05 \text{ Mpc}^{-1}$  [1]. The running spectral index graph is interesting in that it suggests that this model is attempting to emulate both the cutoff at low  $k$ , as well as the reduced power at large  $k$ . The latter is possibly required as the strict power law spectrum at large  $k$  appears to over-predict the abundance of dwarf galaxies. This is discussed further in section 6.

A further quantity of interest is the tensor spectrum, which is significant in searches for B-mode polarisation in the CMB. As our definition of the tensor spectrum we take

$$\mathcal{P}_{\text{grav}}(k) = \frac{16}{\pi} H^2, \quad (81)$$

where again the right-hand side is evaluated as the scale controlled by  $x$  crosses the horizon. (Here we follow the convention of Martin & Schwarz [20]). The main quantity of interest is the ratio of the tensor and scalar modes  $r$ ,

$$r = \frac{\mathcal{P}_{\text{grav}}}{\mathcal{P}_{\mathcal{R}}}, \quad (82)$$

where the right-hand side is evaluated at some suitable low  $k$ . Following the slow-roll approximation, we can write

$$\mathcal{P}_{\text{grav}}(k) = \frac{64\mu^2\phi^2}{3}. \quad (83)$$

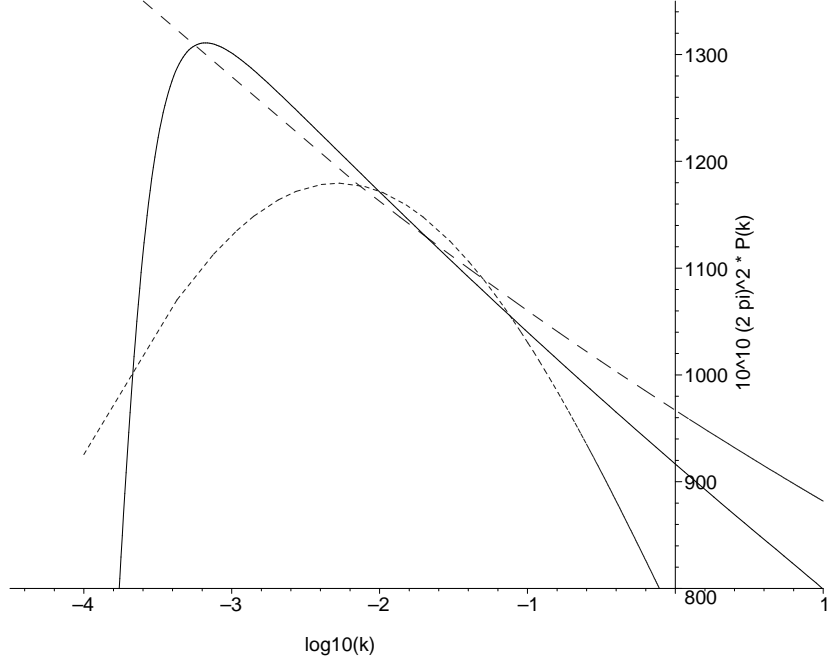


Figure 16: *Comparison of the scalar power spectrum with power law models.* The function plotted is  $10^{10}(2\pi)^2\mathcal{P}_R(k)$  as a function of  $\log_{10}(k)$ , assuming  $h = 0.65$ . The solid line represents the numerical predictions from our model. The long dashes represent the best fit power law ( $n_s = 0.96$ ) and the short dashes are the WMAP running spectral index best fit. Notice that the vertical scale runs from 800 to 1300, so the differences are slightly exaggerated.

Applying  $d/(d \ln k)$  to this now yields

$$\frac{d}{d \ln k} \mathcal{P}_{\text{grav}}(k) = -\frac{32\mu^2}{3\pi}, \quad (84)$$

which is a constant. For the tensor mode spectrum we therefore expect that  $\mathcal{P}_{\text{grav}}$  should be linear in  $\ln(k)$ .

Figure 17 shows the predicted tensor mode perturbation spectrum for our model (again with  $\Omega_0 = 1.02$ ). Also shown (slightly offset) is the best fit model of the form of equation (73), together with an exponential cutoff at low  $k$ . This best fit is given by

$$10^{10} (2\pi)^2 \mathcal{P}_{\text{grav}}(k) = 255(1 - .023 y)(1 - \exp(-(y + 2.6)/0.65)) \quad (85)$$

valid again for  $y > -0.93$ . The slope in this formula is  $255 \times 0.023/(2\pi \times 10^5)^2 = 1.48 \times 10^{-11}$ , which agrees well with the theoretical value of  $32\mu^2/(3\pi) = 1.47 \times 10^{-11}$ . If we form the ratio  $r$  at  $y = 2$ , which corresponds to  $k = 0.0016 \text{ Mpc}^{-1}$  for  $H_0 = 65 \text{ km s}^{-1} \text{ Mpc}^{-1}$ , we find  $r \approx 0.19$ . This is large enough to be detectable in the near future. For example, the predicted sensitivity level to B modes for the Planck satellite corresponds to a detection limit of  $r > 0.05$  [22], comfortably below the value predicted here. A relatively large tensor mode component is therefore a firm prediction of our model.

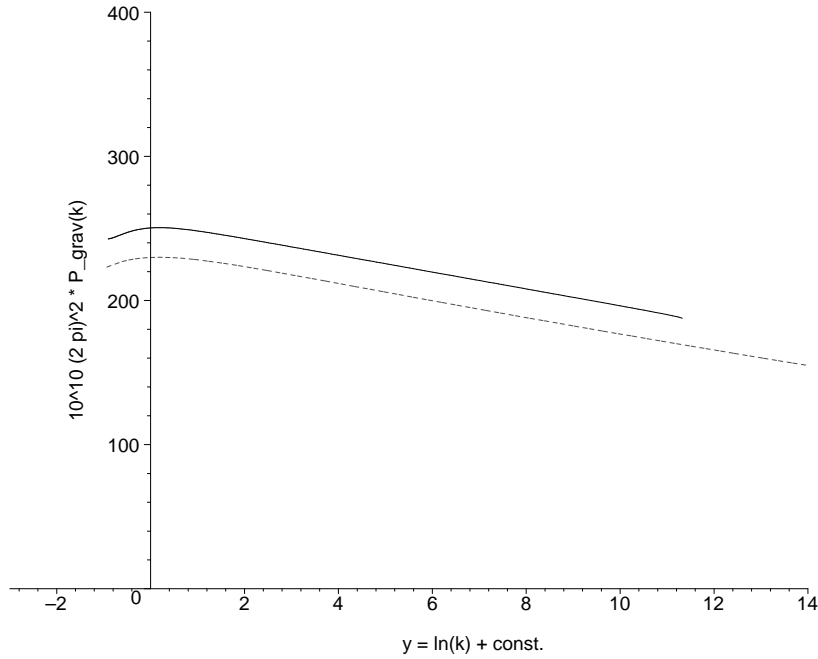


Figure 17: *Power spectrum of tensor perturbations.* The quantity plotted is  $10^{10}(2\pi)^2\mathcal{P}_{\text{grav}}(k)$  versus  $y = \ln(k) + \text{constant}$ . The solid line is the numerical predictions. The dashed line is the best fit power law with exponential cutoff, offset by 20 units vertically for clarity. All parameters are described in the text.

## 6 CMB Power Spectrum and Large Scale Structure

We now turn to using our primordial power spectra to predict the measured fluctuations in the CMB. For this purpose we use the CAMB package [23], which takes as its input the curvature spectrum and various cosmological parameters, and returns the  $C_\ell$  values of the CMB power spectrum. For the cosmological parameters we take  $\Omega_{\text{cdm}}h^2 = 0.135$ ,  $\Omega_{\text{b}}h^2 = 0.0224$  and the optical depth to reionisation  $\tau = 0.17$ . Together with  $\Omega_0 = 1.02$  these correspond to the WMAP best fit values [1]. Additionally, we use a Hubble constant of  $65 \text{ km s}^{-1} \text{ Mpc}^{-1}$ . This is lower than the best fit value quoted WMAP of  $72 \pm 5 \text{ km s}^{-1} \text{ Mpc}^{-1}$ . This latter value is obtained for an assumed *flat* model. If one relaxes the assumption of flatness, then the CMB data is quite degenerate with respect to the values of  $H_0$  and  $\Omega_0$  (see section 6.2 of Spergel et al. [1] for a discussion of this point). Our value of  $H_0 = 65 \text{ km s}^{-1} \text{ Mpc}^{-1}$  is compatible at  $1\sigma$  with virtually all current determinations of  $H_0$ . For example, the HST Key Project value is  $72 \pm 8 \text{ km s}^{-1} \text{ Mpc}^{-1}$  [24], whereas combined Sunyeav–Zel’dovich and X-ray flux measurements consistently favour a slightly lower value [25]. A lower value of  $H_0$  was also suggested for closed models by Efstathiou [21], and our chosen value provides a reasonable fit with the WMAP power spectrum for  $\Omega_0 = 1.02$ . It is worth pointing out in this context that the WMAP simultaneous best fit

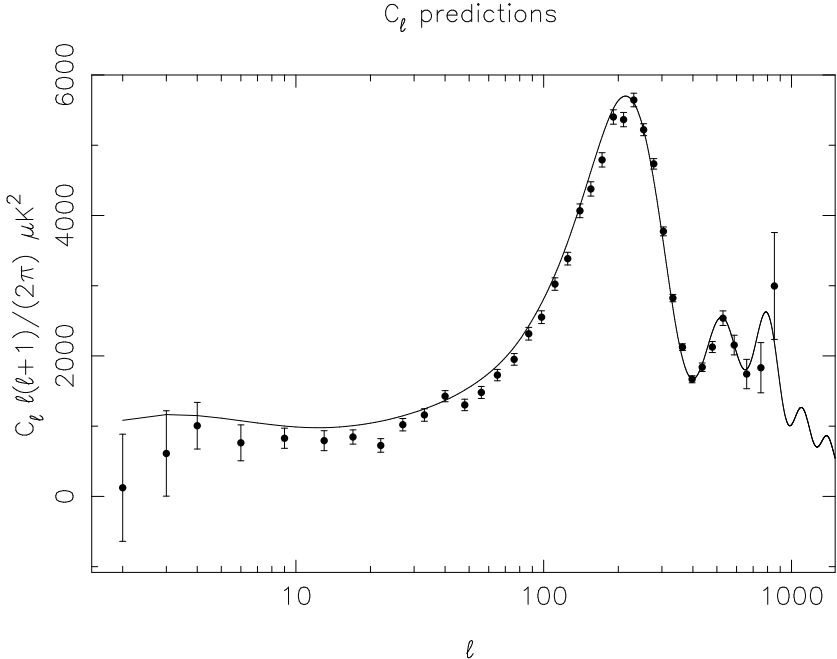


Figure 18: *Predicted CMB power spectrum.* These predictions are for a model with  $\Omega_0 = 1.02$ , as discussed in the text. The experimental points shown with  $1\sigma$  error bars are the WMAP results.

values of  $H_0$  and  $\Omega_0$  actually provide a rather poor fit to their measured CMB spectrum!

In fixing  $\Omega_M$  and  $\Omega_0$  we in turn imply a value of  $\Omega_\Lambda$ . Together these pick out a unique path in the  $\Omega_M$ – $\Omega_\Lambda$  plane, for which we can calculate a total elapsed conformal time. In order to satisfy our boundary condition we need to achieve a value of conformal time by the end of inflation of 0.975. The value of  $b_4/\mu^{4/3}$  is chosen to achieve this. With all the parameters now chosen, the computed CMB power spectrum is shown in figure 18. The fit is reasonably good, particularly at low  $\ell$  where our model does predict a fall off in power.

A further test of our model is the predicted linear matter power spectrum. This is shown in figure 19, where it is compared with the 2dF data of Percival et al. [26]. Also plotted is a fiducial model with  $n_s = 1$ ,  $\sigma_8 = 1$ ,  $h = 0.7$ ,  $\Omega_m h = 0.2$ , and  $\Omega_b = 0$  (and therefore no baryon oscillations). This model is calculated from the fitting formulae of Eisenstein & Hu [27]. In order to achieve a good fit with the data, the vertical scale for our model predictions has been adjusted downwards by about 19%. Clearly, the model we have used so far needs some adjustment in its chosen parameters to correct the normalisation. But here we only wish to compare the overall shapes of the three matter power spectra, leaving the overall normalisation aside. It is clear that the spectrum based on our non-power law primordial spectrum fits the 2dF data with a similar degree of fidelity to the power law-based fiducial model. On large scales (small  $k$ ) both appear to overestimate the 2dF results. This can be explained by the fact that the 2dF results are given convolved with the survey window function, which has

### Matter Power Spectra

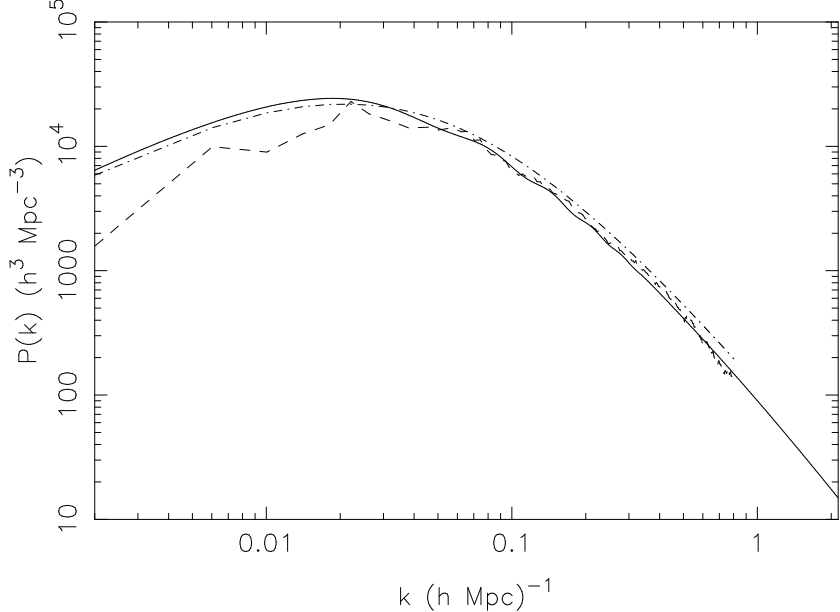


Figure 19: *The linear matter power spectrum.* The solid line is the prediction from CAMB using as input our scalar primordial power spectrum. Long dashes are the 2dF measurements [26] convolved with the survey window function. The dot-dash line is a comparison fiducial model with  $n_s = 1$ ,  $\sigma_8 = 1$ ,  $h = 0.7$ ,  $\Omega_m h = 0.2$ , and  $\Omega_b = 0$ .

its largest effects at large scales (see figure 2 of Percival et al.). On smaller scales our results fit the shape of the 2dF spectrum very well. There is therefore no apparent problem in having a non-power law primordial spectrum right down to these scales. On even smaller scales the relevant comparison would be with Lyman- $\alpha$  data, but this area is still controversial and will not be discussed here.

So far we have developed a model based on the best fit WMAP values for  $\Omega_{\text{cdm}} h^2$ ,  $\Omega_b h^2$  and  $\Omega_0 = 1.02$ , but using a different value of  $H_0$ . This model does provide a reasonable fit, but figure 18 clearly leaves room for improvement, as does the normalisation of the matter spectrum. Ideally we would employ an MCMC analysis to find the best fit parameters for our model, but here we simply give an alternative model which improves the fit. This model has  $\Omega_0 = 1.04$ , so it still consistent with WMAP at the  $1\sigma$  level. We also take  $\Omega_b h^2 = 0.0224$  (as before),  $h = 60$  and  $\Omega_{\text{cdm}} h^2 = 0.110$ . Together these yield a value of  $\Omega_{\text{cdm}} = 0.306$ , which is reasonable. The values of  $b_0$ ,  $b_4$  and  $\mu$  consistent with these are

$$b_0 = 1.64875, \quad \frac{b_4}{\mu^{4/3}} = 0.19791, \quad \mu = 2.1 \times 10^{-6}. \quad (86)$$

The lower value of  $b_4$  produces a universe with larger curvature today. The results of this model are summarised in a best-fit curvature power spectrum

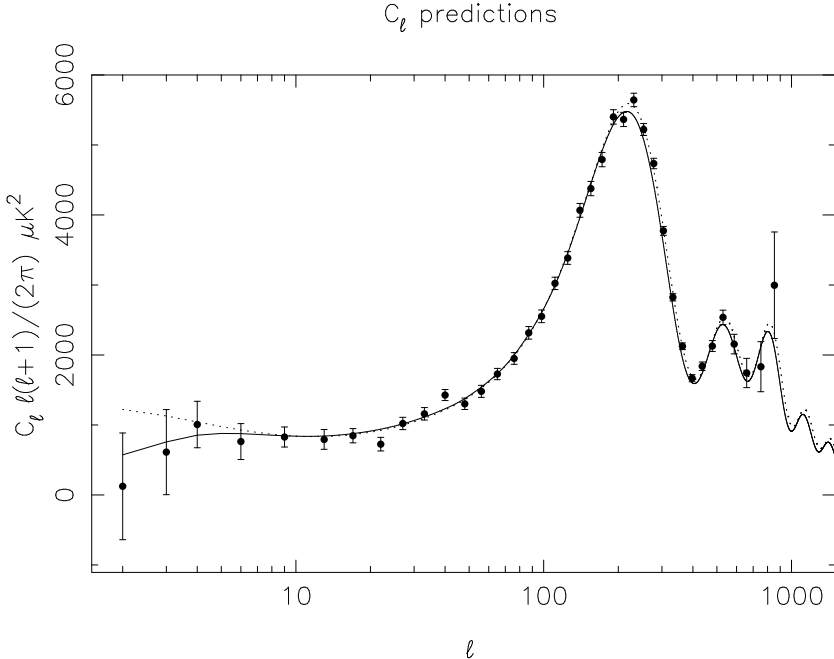


Figure 20: *CMB power spectrum for a model with  $\Omega_0 = 1.04$ .* The parameters are discussed in the text. The experimental points shown with  $1\sigma$  error bars are the WMAP results [1] and the dashed curve corresponds to the best fit  $\Lambda$  CDM power law CMB power spectrum as distributed in the WMAP data products.

given by

$$10^5 2\pi \mathcal{P}_R^{1/2}(k) = 37.55(1 - .023y)(1 - \exp(-(y + 0.20)/0.397)). \quad (87)$$

The result for the CMB power spectrum with these parameters is shown in figure 20. This model clearly gives an extremely good fit to the WMAP spectrum, with the dip at low  $\ell$  now quite pronounced. This is because an increase in  $\Omega_0$  has the effect of sliding the graph to the right in  $k$  space, as is clear from equation (67). The main disadvantage with this model is the low value of  $H_0$ , though this is still within  $1.5\sigma$  of the HST Key Project value.

## 7 Discussion

Many authors have argued that it is difficult to obtain realistic models of a closed inflationary universe [5, 6, 7, 8, 9]. One of the main problems is the low number of e-foldings required, which it is argued demand an unacceptable degree of fine tuning in the initial conditions for inflation. We have shown that this is not the case. It is relatively straightforward to construct inflationary models resulting in a universe which is measurably closed today, using only the simplest model of a free massive scalar field. These models have a number of attractive features and provide a very good fit to the observational data.

One of the reasons we are able to sidestep issues about the initial conditions for inflation is that we run the evolution right back to the big bang. Initial data is specified in terms of two coefficients in the expansion of the scalar field around the initial singularity. This expansion has the notable feature of being a series in both  $t$  and  $\ln(t)$ . We find that the expansion coefficients must both be of order unity to produce evolution consistent with observations. They therefore cannot be said to require much fine tuning.

The predictions of the model are robust against small variations of the input parameters. There is no question of the initial data being specified in a chaotic region of the classical dynamics. Chaotic behaviour in the inflationary equations in a closed universe was noticed by Page [28] and Cornish & Shellard [18]. But these authors considered initial data around  $H = 0$ , whereas our parameters specify the fields as they exit the initial singularity, with  $H = \infty$ . The evolution therefore never enters the region of parameter space where chaotic evolution becomes relevant. The main element of fine tuning required in our model is setting  $\mu = m/m_p$  to  $\approx 10^{-6}$ , but this type of tuning of the potential is a well-known feature of all inflationary theories [16]. Masses of the order of  $10^{-6}m_p$  are quite legitimate from the viewpoint of high-energy physics, which we expect will shed light on the possible origins of such particles.

One of the main novel features of our proposal is the boundary condition we impose on the total conformal time. Based on the conformal representations of closed-universe cosmologies and de Sitter space, we argue that a total conformal time of  $\pi/2$  is naturally picked out on geometric grounds. This gives our model considerable predictive power. For example, given input parameters in the expansion around the big bang, we are able to predict an extremely small cosmological constant, consistent with observation. Imposing boundary conditions at temporal infinity may appear, on the surface, to be a horribly acausal thing to have to do. But we would argue that such a condition is really no different to computing the hydrogen atom bound state spectrum, where boundary conditions are applied at spatial infinity. Furthermore, we hope that our boundary condition will serve as a guide in constructing more detailed physical models of the processes taking place around the big bang.

For those unhappy with our proposed boundary condition, we would point out that many of our conclusions do not depend crucially on it. One can relax the condition, explore the full space determined by the input parameters, and still make sensible predictions about the primordial power spectrum.

Specifying boundary data at the initial singularity and temporal infinity picks out a class of models with a number of desirable features. The universe is closed at around the level of a few percent, and we predict the dip in the CMB power spectrum observed at low  $\ell$ . The statistical significance of this dip has been discussed by many authors [21, 29, 30]. Their main conclusion is that this dip is not inconsistent with the spatially flat concordance model, but could still be an indicator of new physics, provided that any new model does not introduce too many additional parameters. In this respect our model is very efficient. Taking  $\Omega_M$  and  $\Omega_\Lambda$  as input data, the only free parameters are the mass  $\mu$  and the constant  $b_0$ , which controls the number of e-foldings. We also predict a running spectral index with reduced power at high- $\ell$  values. This looks to be favoured by dwarf galaxy and Lyman  $\alpha$  data, though this area is controversial. The behaviour of the CMB spectrum beyond the second peak will also help break degeneracies in various models, and high-resolution

measurements in this region would be extremely valuable.

For our best-fit models we typically predict of the order of 50 e-foldings. Such values are quite natural in our scheme, removing the central objection to closed universes. Furthermore, a value of 50 has the additional feature of removing any potential problems with trans-Planckian physics [16]. That is, there is no question of Planck scale physics being inflated up to cosmological scales. One can see this easily enough by considering the radius of the universe as the inflationary period is entered. We have

$$\frac{R_i}{l_p} \approx \frac{0.5}{\sqrt{|b_4|}} u_i^{1/3} \approx \frac{0.27}{\mu} \frac{1}{b_0^{1/3} (|b_4|/\mu^{4/3})^{1/2}} \quad (88)$$

and, due to the small value of  $\mu$ ,  $R_i$  is already considerably larger than  $l_p$  as inflation starts.

A further indicator that our predictions are relatively insensitive to quantum corrections is provided by equation (48), which gives the value of the total energy in the universe as we leave the big bang. Assuming that  $b_4/\mu^{4/3}$  is of order unity, this expression becomes

$$E_{\text{tot}} \approx \frac{0.03 \hbar}{\mu^2 t}. \quad (89)$$

This tell us that the action  $Et$  is very large, when measured in units of  $\hbar$ . This is reassuring, as it justifies treating the universe on the whole as a classical object. While quantum gravity effects will certainly alter how the universe behaves around the singular region, there is good reason to believe that the predictions of this paper will be largely unaffected by any such new physics.

One further aspect of our model where considerations involving energy are relevant is the end of inflation, as the universe enters a reheating phase. Converting the energy density at the end of inflation into a temperature yields the reasonable value of  $10^{16}$  GeV. This is as expected for typical reheating, if it occurs immediately after inflation is over. But as the scalar field exits inflation the universe is in a matter-dominated phase. Some process has to intervene which converts the scalar field into a radiation-dominated phase. Curiously, this may be difficult to achieve in a way which preserves the total, integrated energy, though there is little difficulty in demanding local conservation. This is probably a reminder that the ‘total energy’ in a closed universe remains a problematic concept in general relativity.

An important question is to identify the main experimental observations which will argue for or against our model. Our first key prediction is the low- $\ell$  dip in the power spectrum. The significance of this could be further enhanced by any lowering of the error bars in these measurements. While cosmic variance is the ultimate determining factor there is still some room for improvement, particularly in the question of foreground contamination [29]. The drop in the power spectrum at large  $\ell$  is also a characteristic feature, which could be detectable with future observations. The third key prediction is the high value of  $r$  — the ratio of tensor to scalar perturbations. This should also be observable by experiments such as the Planck satellite. It would also be of great interest to see which of these predictions is dependent on our choice of potential, and which survive if this restriction is removed.

We hope that much of the future work suggested by this paper is self evident. Before significant future work can begin we need to address the two main

provisos mentioned in the text. The first is that mode quantisation in a closed universe has to be built in. The second is that the mode equations need to be integrated numerically, as aspects of the slow roll approximation are inadequate for our model. Neither of these pieces of work should prove difficult. One area that we aim to address quickly is to explore in more detail the effects of varying the main input parameters, to explore the range of possible universes expected today. One significant point here is that all evolution is constrained to lie inside the matter curve of figure 5. This in itself is a significant restriction. In addition, the parameters chosen for the examples presented here were not computed by detailed model fitting. A full Bayesian determination of these parameters using all available data is clearly desirable, and will give a more stringent test of how well our model holds up.

## Acknowledgements

We thank Anthony Challinor, Anze Slosar, Michael Hobson and other members of the Cambridge–Leverhulme collaboration for useful discussions. CD Thanks the EPSRC for their support.

## A Conformal Line Elements

Here we establish spacetime conformal forms for the standard cosmological line elements for open, closed and flat cosmologies. (The fact that the Weyl tensor vanishes for cosmological models ensures that this is possible.) Our starting point is the FRW line element in the form

$$ds^2 = dt^2 - \frac{R(t)^2}{(1 + kr^2/4)^2} (dr^2 + r^2(d\theta^2 + \sin^2(\theta)d\phi^2)). \quad (90)$$

This line element is already conformal in its spatial component. But a problem with this form is that  $r$  is assumed to be dimensionless. To rectify this we introduce a constant distance  $\lambda$  and replace the line element with

$$ds^2 = dt^2 - \frac{4\lambda^2 R(t)^2}{(\lambda^2 + kr^2)^2} (dr^2 + r^2(d\theta^2 + \sin^2(\theta)d\phi^2)). \quad (91)$$

Here  $t$ ,  $r$ ,  $\lambda$  and  $R$  all have units of distance (assuming  $c = 1$ ). As usual, the constant  $k$  is either  $\pm 1$  or zero.

We seek a coordinate transformation to the spacetime-conformal line element

$$ds^2 = \frac{1}{f^2} (dt^2 - dr^2 - r^2(d\theta^2 + \sin^2(\theta)d\phi^2)), \quad (92)$$

where  $f$  is a (dimensionless) function of  $t$  and  $r$ . Clearly, from the angular terms, we must have

$$\frac{r}{f} = \frac{2\lambda r R(t)}{\lambda^2 + kr^2}. \quad (93)$$

In addition, the coordinate transformation must satisfy

$$\begin{aligned} dt &= f \cosh(u) dt + \frac{r}{r} \sinh(u) dr \\ dr &= f \sinh(u) dt + \frac{r}{r} \cosh(u) dr. \end{aligned} \quad (94)$$

For flat cosmologies ( $k = 0$ ) we simply set  $\mathbf{t}/\lambda$  equal to the conformal time  $\eta$ , with  $\mathbf{r} = r$  and the hyperbolic angle  $u$  set to zero. For non-flat cosmologies it is perhaps surprising to find that  $u$  is non-zero. That is, there is a mismatch between the conformal coordinate frame and the cosmological frame.

The integrability conditions for the coordinate transformation provide a pair of differential equations for  $u$ :

$$r \frac{\partial u}{\partial r} = \sinh(u) \quad (95)$$

$$2\lambda r R(t) \frac{\partial u}{\partial t} = (\lambda^2 + kr^2) \cosh(u) + (-\lambda^2 + kr^2) \quad (96)$$

Equation (95) can be solved straightforwardly to give

$$e^u = \frac{1 + rA(t)}{1 - rA(t)}. \quad (97)$$

The function  $A(t)$  is determined by equation (96), which reduces to

$$2\lambda R \dot{A} = \lambda^2 A^2 + k, \quad (98)$$

where the overdot denotes the derivative with respect to cosmic time  $t$ . The solution for  $A$  depends on the curvature:

$$\lambda A = \begin{cases} \tan(\eta/2) & k = 1 \\ -\tanh(\eta/2) & k = -1. \end{cases} \quad (99)$$

The constant of integration has been chosen such that  $A = 0$  corresponds to  $\eta = t = 0$ .

Next we solve the following pair of equations for  $\mathbf{r}$ :

$$r \frac{\partial \mathbf{r}}{\partial r} = \mathbf{r} \cosh(u), \quad \frac{\partial \mathbf{r}}{\partial t} = f \sinh(u). \quad (100)$$

With a suitable choice of the arbitrary scale factor we find that

$$\mathbf{r} = \frac{\lambda^2 A^2 / k + 1}{1 - r^2 A^2} r. \quad (101)$$

The remaining equations determining  $\mathbf{t}$  are

$$r \frac{\partial \mathbf{t}}{\partial r} = \mathbf{r} \sinh(u), \quad \frac{\partial \mathbf{t}}{\partial t} = f \cosh(u). \quad (102)$$

These are solved by

$$\mathbf{t} = \frac{\lambda^2 + kr^2}{1 - r^2 A^2} \frac{A}{k}. \quad (103)$$

Here the arbitrary constant of integration has been fixed to ensure that  $t = \eta = 0$  corresponds to  $\mathbf{t} = 0$ .

With  $\mathbf{r}$  and  $\mathbf{t}$  now found, we can write

$$f = \frac{\lambda^2 A^2 + k}{2\lambda A R} \mathbf{t}. \quad (104)$$

Our remaining task is to find an expression for  $t$  in terms of  $t$  and  $r$ . For this we use that result that

$$\frac{2\lambda t}{\lambda^2 + k(r^2 - t^2)} = \frac{2\lambda A}{k - \lambda^2 A^2}. \quad (105)$$

The right-hand side is now a function of  $t$  only, so the left-hand side can be used in place of cosmic time. Again, the explicit form depends on the cosmology. For spatially closed cosmologies we can write

$$\frac{2\lambda t}{\lambda^2 + r^2 - t^2} = \tan(\eta) \quad (106)$$

whereas for spatially open we have

$$\frac{2\lambda t}{\lambda^2 + t^2 - r^2} = \tanh(\eta). \quad (107)$$

The three cosmological scenarios can now be summarised as

$$\begin{aligned} f &= \frac{t}{R \sin(\eta)} = g \left( \frac{2\lambda t}{\lambda^2 + r^2 - t^2} \right) \frac{t}{\lambda} && \text{closed} \\ f &= \frac{2\lambda}{R} && \text{flat} \\ f &= \frac{t}{R \sinh(\eta)} = \bar{g} \left( \frac{2\lambda t}{\lambda^2 + t^2 - r^2} \right) \frac{t}{\lambda} && \text{open} \end{aligned} \quad (108)$$

which are the results used in the main text.

## References

- [1] D.N. Spergel et al. First year Wilkinson anisotropy probe (WMAP) observations: Determination of cosmological parameters. *ApJ*, To Appear, 2003.
- [2] D.A. Brannan, M.F. Espleen, and J.J. Gray. *Geometry*. Cambridge University Press, 1999.
- [3] C.J.L Doran and A.N. Lasenby. *Geometric Algebra for Physicists*. Cambridge University Press, 2003.
- [4] A.N. Lasenby. Conformal geometry and the universe. *Phil. Trans. R. Soc. Lond. A*, to appear, 2003.
- [5] A. Linde. Can we have inflation with  $\Omega > 1$ ? astro-ph/0303245, 2003.
- [6] A.A. Starobinsky. Spectrum of initial perturbations in open and closed universes. In M. Khlopov, M.E. Prokhorov, A.A. Starobinsky, and J. Tran Thanh Van, editors, *Cosmoparticle Physics*, page 43. Edition Frontiers, 1996.
- [7] J. Uzan, U. Kirchner, and G.F.R. Ellis. WMAP data and the curvature of space. astro-ph/0302597, 2003.

- [8] G.F.R. Ellis, W. Stoeger, P. McEwan, and P. Dunsby. Dynamics of inflationary universes with positive spatial curvature. *Gen.Rel.Grav.*, 34:1445, 2002.
- [9] G.F.R. Ellis, P. McEwan, W. Stoeger, and P. Dunsby. Causality of inflationary universes with positive spatial curvature. *Gen.Rel.Grav.*, 34:1461, 2002.
- [10] C.J. Isham and J.E. Nelson. Quantization of a coupled Fermi field and Robertson-Walker metric. *Phys. Rev. D*, 10(10):3226, 1974.
- [11] A.N. Lasenby, C.J.L. Doran, and S.F. Gull. Gravity, gauge theories and geometric algebra. *Phil. Trans. R. Soc. Lond. A*, 356:487–582, 1998.
- [12] N.A. Chernikov and E.A. Tagirov. Quantum theory of scalar fields in de Sitter space-time. *Ann. Inst. Henri Poincaré*, 9A:109, 1968.
- [13] N.D. Birrell and P. C. W. Davies. *Quantum Fields in Curved Space*. Cambridge University Press, 1982.
- [14] B. Allen. Vacuum states in de Sitter space. *Phys. Rev. D*, 32:3136, 1985.
- [15] U.H. Danielsson. Inflation, holography, and the choice of vacuum in de Sitter space. *J. High Energy Phys.*, 07:40, 2002.
- [16] R.H. Brandenberger. Principles, progress and problems in inflationary cosmology. *AAPPS Bull.*, 11:20, 2001.
- [17] W. Greiner. *Relativistic Quantum Mechanics*. Springer-Verlag, Berlin, 1990.
- [18] N. Cornish and E.P.S. Shellard. Chaos in quantum cosmology. *Phys. Rev. Lett.*, 81:3571, 1998.
- [19] A.R. Liddle and D.H. Lyth. *Cosmological Inflation and Large-Scale Structure*. Cambridge University Press, 2000.
- [20] J. Martin and D.J. Schwarz. The precision of slow-roll predictions for the CMBR anisotropies. *Phys.Rev.*, D62:103520, 2000.
- [21] G. Efstathiou. Is the low CMB quadrupole a signature of spatial curvature? *astro-ph/0303127*, 2003.
- [22] G. Franco, P. Fosalba, and J.A. Tauber. Systematic effects in the measurement of polarization by the PLANCK telescope. *astro-ph/0210109*, 2002.
- [23] A.M. Lewis, A.D. Challinor, and A.N. Lasenby. Efficient computation of CMB anisotropies in closed FRW models. *Ap. J.*, 538:473, 2000.
- [24] W.L. Freedman et al. Final results from the Hubble space telescope key project to measure the Hubble constant. *Ap. J.*, 553:47, 2001.
- [25] M.E. Jones et al.  $H_0$  from an orientation-unbiased sample of SZ and X-ray clusters. *astro-ph/0103046*, 2001.

- [26] W.J. Percival et al. The 2dF galaxy redshift survey: The power spectrum and the matter content of the universe. *MNRAS*, 327:1297, 2001.
- [27] D.J. Eisenstein and W. Hu. Baryonic features in the matter transfer function. *Ap. J.*, 496:605, 1998.
- [28] D.N. Page. A fractal set of perpetually bouncing universes. *Class. Quant. Grav.*, 1:417, 1984.
- [29] G. Efstathiou. The statistical significance of the low CMB multipoles. astro-ph/0306431, 2003.
- [30] C.R. Contaldi, M. Peloso, L. Kofman, and A. Linde. Suppressing the lower multipoles in the CMB anisotropies. astro-ph/0303636, 2003.